

# The Segmented Zambezi Sedimentary System from Source to Sink

## 1. Sand Petrology and Heavy Minerals

*Eduardo Garzanti<sup>1,\*</sup>, Guido Pastore<sup>1</sup>, Alberto Resentini<sup>1</sup>, Giovanni Vezzoli<sup>1</sup>, Pieter Vermeesch<sup>2</sup>,  
Lindani Ncube<sup>3</sup>, Helena Johanna Van Niekerk<sup>3</sup>, Gwenael Jouet<sup>4</sup>, Massimo Dall'Asta<sup>5</sup>*

<sup>1</sup>*Laboratory for Provenance Studies, Department of Earth and Environmental Sciences, University of Milano-Bicocca, 20126 Milano, Italy*

<sup>2</sup>*London Geochronology Centre, Department of Earth Sciences, University College London, London, WC1E 6BT, UK*

<sup>3</sup>*Department of Environmental Sciences, University of South Africa, Florida, South Africa*

<sup>4</sup>*Unité de Recherche Géosciences Marines, Ifremer, CS 10070, 29280 Plouzané, France*

<sup>5</sup>*TOTAL E&P, CSTJF, Avenue Larribau - 64018 Pau Cedex Pau, France*

Email: [eduardo.garzanti@unimib.it](mailto:eduardo.garzanti@unimib.it) (Garzanti), [g.pastore2@campus.unimib.it](mailto:g.pastore2@campus.unimib.it) (Pastore), [alberto.resentini@unimib.it](mailto:alberto.resentini@unimib.it) (Resentini), [giovanni.vezzoli@unimib.it](mailto:giovanni.vezzoli@unimib.it) (Vezzoli), [p.vermeesch@ucl.ac.uk](mailto:p.vermeesch@ucl.ac.uk) (Vermeesch), [ncubel@unisa.ac.za](mailto:ncubel@unisa.ac.za) (Ngube), [vniekhj@unisa.ac.za](mailto:vniekhj@unisa.ac.za) (Van Niekerk), [gwenael.jouet@ifremer.fr](mailto:gwenael.jouet@ifremer.fr) (Jouet), [massimo.dallasta@total.com](mailto:massimo.dallasta@total.com) (Dall'Asta)

**Key words:** Sedimentary petrology; Heavy minerals; Anorogenic volcanic provenance; Continental block provenance; Weathering and recycling; Drainage evolution; Transmission of provenance signals; African landscape

## ABSTRACT

The Zambezi River rises at the center of southern Africa, flows across the low-relief Kalahari Plateau, meets Karoo basalt, plunges into Victoria Falls, follows along Karoo rifts, and pierces through Precambrian basement to eventually deliver its load onto the Mozambican passive margin. Reflecting its polyphase evolution, the river is subdivided into segments with different geological and geomorphological character, a subdivision finally fixed by man's construction of large reservoirs and faithfully testified by sharp changes in sediment composition. Pure quartzose sand recycled from Kalahari desert dunes in the uppermost tract is next progressively enriched in basaltic rock fragments and clinopyroxene. Sediment load is renewed first downstream Lake Kariba and next downstream Lake Cahora Bassa, documenting a stepwise decrease in quartz and durable heavy minerals. Composition becomes quartzo-feldspathic in the lower tract, where most sediment is supplied by high-grade basements rejuvenated by the southward propagation of the East African rift. Feldspar abundance in Lower Zambezi sand has no equivalent among big rivers on Earth and far exceeds that in sediments of the northern delta, shelf, and slope, revealing that provenance signals from the upper reaches have ceased to be transmitted across the routing system after closure of the big dams. This high-resolution petrologic study of Zambezi sand allows us to critically reconsider several dogmas, such as the supposed increase of mineralogical "maturity" during long-distance fluvial transport, and forges a key to unlock the rich information stored in sedimentary archives, with the ultimate goal to accurately reconstruct the evolution of this mighty river flowing across changing African landscapes since the late Mesozoic.

“A river or a drainage basin might best be considered to have a heritage rather than an origin. It is like an organic form, the product of a continuous evolutionary line through time.”

*Leopold et al. 1995, p.421*

“Nyaminyami is a personification of the Zambezi itself and, by analogy, of the life force and the will to survive.”

*Main 1990, ZAMBEZI Journey of a river, ch.8, p.124*

## Introduction

1

2

3 The Zambezi is one of the most fascinating river systems on Earth, flowing across wild landscapes  
4 from Barotseland to Victoria Falls and next plunging into deep gorges carved in basalt and along  
5 ancient rift valleys to finally reach the Indian Ocean (Fig. 1; Main 1990; Moore et al. 2007). The  
6 relatively recent, complex and controversial natural evolution of its drainage basin ended in the  
7 Anthropocene with its drastic subdivision into separate segments by man’s construction of two big  
8 dams and associated reservoirs.

9 This is the first of a series of articles aiming at characterizing, by a multitechnique approach, the  
10 composition of sediment generated in the diverse tracts of the vast Zambezi catchment and the present  
11 and inherited factors that influence compositional variability from the headwaters to the Mozambican  
12 coast and beyond. This study, based on framework petrography and heavy-mineral data, focusses  
13 specifically on: a) the relative effects of source-rock lithology and chemical weathering on sand  
14 mineralogy in a subequatorial climate; b) the transmission of compositional signals along the  
15 sediment-routing system from source to sink; c) the use and misuse of current petrological models to  
16 infer sediment provenance and of mineralogical parameters to infer climatic conditions. A  
17 forthcoming companion paper will be based on complementary data from sand and mud  
18 geochemistry, clay mineralogy, and detrital zircon geochronology on the same sample set (Garzanti  
19 et al., forthcoming). Our ultimate purpose is to build up a solid knowledge of the modern sedimentary  
20 system that can be applied to trace fluvial transport from the land to the deep sea and, eventually, to

21 investigate provenance changes recorded in stratigraphic successions accumulated in marine  
22 depocentres through time and thus unravel the complex evolution of the Zambezi River since the late  
23 Mesozoic.

24

25

## Geology

26

27 *The Precambrian.* The Archean core of southern Africa includes the Zimbabwe Craton, welded  
28 by the Limpopo Belt to the Kaapvaal Craton in the south and bounded by the mid-Paleoproterozoic  
29 Magondi Belt in the west (Fig. 2). The Zimbabwe Craton comprises a central terrane flanked by  
30 greenstone belts. Gneisses of the central terrane are non-conformably overlain by volcanic rocks and  
31 conglomerates. The craton was stabilized in the mid-Neoproterozoic and finally sealed by the Great Dyke  
32 swarm at ~2575 Ma (Jelsma and Dirks 2002; Söderlund et al. 2010).

33 The composite Archean core grew progressively during the Paleoproterozoic and Mesoproterozoic.  
34 The Proto-Kalahari Craton was established by the late Paleoproterozoic and affected by widespread  
35 intraplate magmatism at 1.1 Ga (Hanson et al. 2006), not long before the Kalahari Craton was formed  
36 during the orogenic event when Rodinia was assembled (Jacobs et al. 2008).

37 Orogens developed in the Paleoproterozoic and reworked in the Neoproterozoic at the southern margin  
38 of the Tanzania Craton include the NW/SE trending Ubendian metamorphic belt, bounding the  
39 Bangweulu Block to the north (Boniface and Appel 2018) and the SW/NE striking Usagaran Belt to  
40 the east (Collins et al. 2004). In northern Zimbabwe, the Orosirian Magondi Belt contains arc-related  
41 volcano-sedimentary and plutonic rocks metamorphosed at amphibolite facies (Majaule et al. 2001;  
42 Master et al. 2010).

43 Orogens generated in the Mesoproterozoic include the Kibaran Belt in the north (Kokonyangi et al.  
44 2006; Debruyne et al. 2015) and the Irumide Belt, which stretches from central Zambia in the SW to  
45 northern Malawi in the NE, is delimited by the largely undeformed basement of the Bangweulu block  
46 in the north, and was largely affected by the Neoproterozoic orogeny in the west (Fig. 2). The Irumide

47 Belt includes a Paleoproterozoic gneissic basement overlain by siliciclastic and minor carbonate strata  
48 deposited during the late Orosirian (Muva Supergroup), as well as granitoid suites emplaced in the  
49 earliest, middle, and latest Mesoproterozoic. During the ~1 Ga orogeny, metamorphic grade increased  
50 from greenschist facies in the NW to upper amphibolite and granulite facies in the SE (De Waele et  
51 al. 2006, 2009). The Choma–Kalomo block in southern Zambia is a distinct Mesoproterozoic domain  
52 also including amphibolite-facies metasediments and granitoid intrusions affected by the latest  
53 Mesoproterozoic thermal event (Glynn et al. 2017).

54 The Kalahari Craton of southern Africa was finally welded to the Congo Craton during the major  
55 Neoproterozoic Pan-African orogeny, testified by the Damara–Lufilian–Zambezi Belt stretching  
56 from coastal Namibia in the west and across Botswana and southern Zambia to finally connect with  
57 the Mozambique Belt in the east (Frimmel et al. 2011; Fritz et al. 2013; Goscombe et al. 2020). The  
58 Lufilian Arc, located between the Congo and Kalahari Cratons, consists of Neoproterozoic low- to  
59 high-grade metasedimentary and metaigneous rocks hosting Cu-Co-U and Pb-Zn mineralizations  
60 (Kampunzu and Cailteux 1999; John et al. 2004; Eglinger et al. 2016). The Zambezi Belt contains a  
61 volcano-sedimentary succession deformed under amphibolite-facies conditions during the early  
62 Neoproterozoic (Hanson 2003), whereas eclogite-facies metamorphism constrains the timing of  
63 subduction and basin closure as latest Neoproterozoic (Hargrove et al. 2003; John et al. 2003).

64 *The break-up of Gondwana.* A major tectono-magmatic event straddling the  
65 Paleozoic/Mesozoic boundary is widely documented across southern Africa (Jourdan et al. 2005;  
66 Manninen et al. 2008), when the several km-thick Upper Carboniferous to Lower Jurassic Karoo  
67 Supergroup was deposited, including glacial sediments, shale, and volcanoclastic sandstone followed  
68 by fluvial sediments (Johnson et al. 1996). Sedimentation was influenced by changing climate, from  
69 initially cold to warmer since the mid-Permian and finally hot with fluctuating precipitation in the  
70 Triassic, when braidplain sandstone and floodplain mudstone were capped by eolian sandstone  
71 (Catuneanu et al. 2005). Karoo-type basins formed in intra- and inter-cratonic settings by rift-related

72 extension. In the Tuli and Mid-Zambezi basins of Zimbabwe, glacial deposits are overlain by Permian  
73 sandstones and coal-bearing mudrocks, followed by ~0.5-km-thick Triassic redbeds and pebbly  
74 sandstones (Bicca et al. 2017). Karoo sedimentation was terminated by flood-basalt eruptions  
75 recorded throughout southern Africa in the Early Jurassic (Svensen et al. 2012).  
76 Finally, rifting and break-up of Gondwana in the mid-Jurassic was followed by opening of the Indian  
77 Ocean in the Early Cretaceous, an event associated with formation of sedimentary basins (Salman  
78 and Abdula 1995; Walford et al. 2005), strike-slip deformation (Klimke et al. 2016), and extensive  
79 volcanism in the Mozambique Channel (Vallier et al. 1974; König and Jokat 2010).  
80 In the Cenozoic, fluvial and lacustrine sediments were deposited inland in the Mega-Kalahari rim  
81 basin (in Tswana language *Kgalagadi*, “waterless place”), which comprises the largest sand sea on  
82 Earth extending across the southern Africa plateau for over  $2.5 \cdot 10^6$  km<sup>2</sup> (Haddon and McCarthy  
83 2005). Repeated phases of eolian deposition took place during Quaternary dry stages, separated by  
84 depositional hiatuses corresponding to more humid stages (Stokes et al. 1998; Thomas and Shaw  
85 2002). The East African rift developed throughout the Neogene (Ebinger and Scholz 2012; Roberts  
86 et al. 2012; Maselli et al. 2019), until along-axis propagation reached the Kalahari region in the  
87 Quaternary, through a network of unconnected basins extending SW of Lake Tanganyika (Kinabo et  
88 al. 2007). Since the late Pleistocene, faulting and subsidence in the incipient Okavango rift zone has  
89 exerted a major control on drainage reorganization.

## 91 The Zambezi River

92  
93 The Zambezi (from either the Bantu term *mbeze*, “fish”, or the M’biza people of central-eastern  
94 Zambia), 2575 km in length and with a catchment area of  $\sim 1.4 \cdot 10^6$  km<sup>2</sup>, is the largest river of southern  
95 Africa, extending from 11°S to 20°S and from 19°E to 36°30’E (Fig. 1). Annual water discharge is  
96  $\sim 100$  Km<sup>3</sup>, and suspended load amounts to 50-100 million tons (Hay 1998). Annual rainfall in the  
97 basin increases from < 600 mm in the south to > 1200 mm in the north. The largest contribution to

98 runoff, therefore, comes from the headwater branches in Zambia and Angola. Mean monthly flows  
99 at Victoria Falls remain over 1000 m<sup>3</sup>/s from February to June, with maxima of 3000 m<sup>3</sup>/s in April  
100 and minima of 300 m<sup>3</sup>/s in October to November; 9000 m<sup>3</sup>/s were reached during the 1958 flood,  
101 while the Kariba Dam was under construction (Moore et al. 2007).

102 The natural course of the Zambezi River has been modified profoundly by the great dams that have  
103 created since 1959 Lake Kariba, marking the border between Zimbabwe and Zambia, and since 1974  
104 Lake Cahora Bassa in northern Mozambique (the former site of the frightful impassable rapids named  
105 *kebrabassa*, “end of work”, by slaves who could proceed no farther upstream). Because the sediment-  
106 routing system is strictly partitioned by these two major reservoirs, it is here convenient to distinguish  
107 four reaches: a) an uppermost Zambezi headwater tract as far as the Kwando confluence; b) an Upper  
108 Zambezi that includes Victoria Falls and the Batoka Gorge as far as Lake Kariba; c) a Middle Zambezi  
109 between the two reservoirs; d) a Lower Zambezi downstream of Lake Cahora Bassa (Fig. 3).

110 Sourced among low ridges of the Kasai Shield in the Mwinilunga District of northernmost Zambia  
111 and undecided at first whether to head towards the Atlantic or Indian Ocean, the Uppermost Zambezi  
112 cuts across Precambrian basement in easternmost Angola. Back to Zambia, the river traverses  
113 unconsolidated Kalahari sands and widens in a ~180 km-long floodplain reaching 30 km in width  
114 during peak flood (O'Connor and Thomas 1999). Tree growth is inhibited by the persistently high  
115 water table and river waters slowly filter through the wetland, where clay accumulates in soils  
116 enriched in humus.

117 The major Uppermost Zambezi tributary is the Kwando River. Sourced in humid Angola, which  
118 receives an annual precipitation up to 1400 mm concentrated between December and March when  
119 the southward migration of the Congo Air Boundary brings heavy rains, the river chiefly drains the  
120 vegetated Mega-Kalahari dune field (Shaw and Goudie 2002). After entering the Okavango Rift  
121 (Modisi et al. 2000; Kinabo et al. 2007), the Kwando (here named Linyanti, and next Chobe) deviates  
122 sharply eastward along the Linyanti and Chobe Faults, forming a tectonic depression that favored the

123 recent capture of the Kwando by the Zambezi and is presently favoring the capture of Okavango  
124 waters as well, conveyed eastward along the Selinda spillway (Gumbrecht et al. 2001). The  
125 depression, hosting large swamps and once large paleolakes (Shaw and Thomas 1988), continues into  
126 Zambia, where it includes the low-gradient Kasaya and Ngwezi Rivers. These west-bank tributaries  
127 of the Zambezi, as the Kabombo (Kabompo) to the north, are sourced in the Lufilian Arc.  
128 Downstream of the Kwando confluence, the Upper Zambezi and its local tributaries (e.g., Sinde from  
129 Zambia) incise into Karoo basaltic lavas, where the gradient steepens forming local rapids. Suddenly,  
130 the river plunges some 100 m along the 1.7 km length of the Victoria Falls (in Lozi language *Mosy-*  
131 *wa-Tunya*, “the-Smoke-that-Thunders”), and the turbulent waters downstream carve an amazing  
132 zigzag into the deep Batoka Gorge of black Karoo basalt, the result of progressive retreat of the  
133 waterfalls during the Quaternary (Derricourt 1976). After receiving tributaries draining Karoo lavas  
134 overlain by a veneer of Kalahari dune sand (Masuie and Matetsi from Zimbabwe), the river reaches  
135 Lake Kariba shortly downstream of the confluence with the Gwai River. The senile low-gradient  
136 upper reaches of this major tributary sourced in the Zimbabwe Craton are incised, as its east-bank  
137 sub-tributaries, in Karoo basalt and sedimentary rocks surrounded by Kalahari dune sand (Thomas  
138 and Shaw 1988; Moore et al. 2009a), whereas the youthful lower reaches cut steeply across the  
139 Paleoproterozoic basement of the Magondi Belt (Fig. 3).

140 In the lower 1400 km, the Zambezi skirts around the Zimbabwe Craton, flowing through a rift zone  
141 formed on top of the Pan-African (Kuunga) suture zone (Goscombe et al. 2020) and hosting a thick  
142 infill of Karoo sediments and lavas (Nyambe and Utting 1997). The major north-bank Zambian  
143 tributaries of the Middle Zambezi are the Kafue and the Luangwa Rivers. The Kafue drains southward  
144 into the Lufilian Arc and next turns sharply eastwards, cutting across the Zambezi Belt to eventually  
145 reach the Zambezi mainstem (Fig. 3). The Luangwa, sourced in the Ubendian Belt of northernmost  
146 Zambia, flows for most of its course along a Karoo rift basin filled with an 8 km-thick Permo-Triassic



147 sedimentary succession ([Banks et al. 1995](#)), and finally traverses the Zambezi Belt before joining the  
148 Zambezi just upstream of Lake Cahora Bassa.

149 Major tributaries in Mozambique are the Mazowe (Mazoe) and Luenha (Luia), sourced in the  
150 Zimbabwe Craton to the west, and the Shire, the outlet of Lake Malawi (Nyassa). Most detritus  
151 contributed by tributaries joining the trunk river from either side is generated from upper  
152 Mesoproterozoic gneissic basement reworked during the Neoproterozoic Pan-African orogeny  
153 ([Grantham et al. 2011](#)). Minor tributaries (e.g., Minjova) and sub-tributaries in the north drain also  
154 the Karoo Supergroup ([Fernandes et al. 2015](#)).

155 Finally, the Lower Zambezi traverses the Cretaceous and Cenozoic sedimentary covers of the  
156 Mozambique lowlands ([Fig. 2](#)). Here the river forms a large floodplain with multiple meandering  
157 channels, oxbow lakes and swamps before emptying into the Indian Ocean, where it feeds a wide  
158 shelf extending beyond Beira in the south and Quelimane in the north. The flatness of the shelf,  
159 reaching 150 km in width offshore Beira, contributes to the highest tidal range around Africa (up to  
160 6.4 m).

161 The finest sediment fractions of the river suspended load settle far off the shelf, forming a wide mud  
162 apron on the slope between 300 and 2000 m water depth. A considerable fraction of Zambezi  
163 sediment, however, is not deposited today offshore of the mouth, but transported towards the north-  
164 east, a direction opposite to the mean flow within the Mozambique Strait ([Schulz et al. 2011](#); [van der  
165 Lubbe et al. 2014](#)). Longshore currents are confined to the the inner shelf, whereas the outer shelf is  
166 largely covered by palimpsest sand with heavy-mineral lags formed by winnowing by strong oceanic,  
167 tidal, and wave-induced currents ([Beiersdorf et al. 1980](#); [Miramontes et al. 2020](#)).

168 The multi-sourced Zambezi deep-sea fan, one of the Earth's largest turbidite systems active since the  
169 Oligocene ([Droz and Mougnot 1987](#)), is mainly fed via the ~1200 km-long, curvilinear, and  
170 exceptionally wide Zambezi Valley starting at the shelfbreak offshore Quelimane ~200 km NE of the

171 Zambezi mouth (Fig. 1). In the over 1000 km-long fan, up to very-coarse-grained sand occurs from  
172 the upper canyon to the distal lobes (Kolla et al. 1980; Fierens et al. 2019, 2020).

173 ***Drainage evolution.*** The history of the Zambezi River reflects the multistep changes of African  
174 landscape caused by the progressive break-up of Gondwana (Partridge and Maud 1987; Key et al.  
175 2015; Knight and Grab 2018). Extensional phases in eastern southern Africa started in the Permian  
176 (Macgregor 2018). The entire Middle Zambezi and its major tributary the Luangwa River flow along  
177 Permo-Triassic rift zones (Fig. 2). The eastward slope, instead, originated in the Early Cretaceous by  
178 domal uplift related to incipient rifting of the South Atlantic and emplacement of the Paranà-Etendeka  
179 large igneous province in the west (Cox 1989; Moore and Blenkinsop 2002). Superposed onto  
180 Precambrian mobile belts and Permo-Triassic rifts, or intersecting them, the southward propagation  
181 of the East African Rift during the Neogene has created further tectonic depressions, including those  
182 occupied by Lake Malawi in the east and by the Okavango inland delta in the west (Ebinger and  
183 Scholz 2012). The modern Zambezi drainage is thus the result of inheritance from multiple Permo-  
184 Mesozoic extensional events on both sides of Africa combined with rifting inside Africa that is still  
185 ongoing.

186 Successive events of river capture and drainage reversal, indicated by sharp changes in direction of  
187 its major Kwando, Kafue and Luangwa tributaries, and the genetic similarities of fish populations  
188 between the Kafue and Upper Zambezi, and between the Middle Zambezi and the Limpopo, have  
189 long suggested that the Zambezi, Okavango and Limpopo originally formed a single transcontinental  
190 river following uplift associated with Early Cretaceous rifting of the South Atlantic (Thomas and  
191 Shaw 1988; Moore et al. 2007). In the Paleogene, uplift of the Ovamboland-Kalahari-Zimbabwe axis  
192 resulted in endorheic drainage of the Okavango and upper Zambezi (Moore and Larkin 2001). The  
193 then isolated Lower Zambezi initiated headward erosion, leading to the sequential capture of its  
194 middle- and upper-course tributaries. Both Kafue and Luangwa Rivers once drained southwestward,  
195 the former joining the Upper Zambezi in the Machili Flats and the latter flowing across the Gwembe

196 trough presently occupied by Lake Kariba (Thomas and Shaw 1991). Linking with the upper course  
197 in the Plio-Pleistocene was followed by the capture of the Kwando River, and by the presently  
198 occurring capture of the Okavango as well (Wellington 1955; Moore et al. 2007). In NW Zimbabwe,  
199 drainage is largely controlled by an old pre-Karoo surface, tilted westward during domal uplift in the  
200 Early Jurassic (Moore et al. 2009a). The present east-bank tributaries of the Gwai River all drained  
201 westwards toward Botswana, until they were captured by headward erosion of the Gwai River after  
202 establishment of the modern Zambezi river course (Thomas and Shaw 1988).

203

204

### Methods

205

206 Between 2018 and 2019, we collected 31 sediment samples ranging in size from very fine to coarse  
207 sand from active river bars of the Zambezi River and of its major tributaries in Zambia and  
208 Mozambique. In 2011, 25 additional sediment samples were collected in the Zambezi, Kwando, and  
209 Gwai catchments in Zambia, Caprivi Strip, Botswana, and Zimbabwe. To cover the entire Zambezi  
210 system from source to sink, we also studied four fine sands from the Bons Sinais Estuary and adjacent  
211 beaches in the Quelimane area of the northern Zambezi delta, and five sandy silts collected offshore  
212 of Quelimane (core MOZ4-CS14, 181 m b.s.l.) and of the Zambezi delta (core MOZ4-CS17; 550 m  
213 b.s.l.) during the PAMELA-MOZ04 Ifremer-Total survey (Jouet and Deville 2015). Offshore  
214 sediments, collected by Calypso piston corer within 25 m below the sea floor, were deposited during  
215 the last glacial lowstand (MOZ4-CS17-2402-2407cm, 24.1 ka), the post-glacial warming and sea-  
216 level rise (MOZ4-CS14-1602-1607cm, 15.9 ka; MOZ4-CS17-702-707cm, 14.6 ka), and the  
217 Holocene highstand (MOZ4-CS14-21-26cm, 4.3 ka; MOZ4-CS17-52-57cm, 4.0 ka). These  
218 sediments were dated using accelerator mass spectrometer (AMS) standard radiocarbon methods on  
219 marine mollusk shells and bulk assemblages of planktonic foraminifera by applying a local marine  
220 reservoir correction of mean  $\Delta R = 158 \pm 42$  yr. Analyses, calibrated dates, and interpolated age

221 models are illustrated in detail in [Zindorf et al. \(2021\)](#). Full information on sampling sites is provided  
222 in [Appendix Table A1](#) and Google Earth® file [Zambezi.kmz](#).

223 **Petrography.** A quartered fraction of each sample was impregnated with Araldite® resin, stained  
224 with alizarine red to distinguish dolomite and calcite, cut into a standard thin section, and analysed  
225 by counting 400 or 450 points by the Gazzi-Dickinson method ([Ingersoll et al. 1984](#)). Sand is  
226 classified according to the three main groups of framework components (Q = quartz; F = feldspars;  
227 L = lithic fragments), considered where exceeding 10%QFL and listed in order of abundance  
228 (classification scheme after [Garzanti 2019](#)). Feldspatho-quartzose sand is thus defined as  $Q > F >$   
229  $10\%QFL > L$ , formally distinguishing between feldspar-rich ( $Q/F < 2$ ) and quartz-rich ( $Q/F > 4$ )  
230 compositions. Pure quartzose sand is defined as  $Q/QFL > 95\%$ . These distinctions proved to be  
231 essential to discriminate among lithic-poor siliciclastic sediments generated from cratonic blocks and  
232 deposited along passive continental margins in different geomorphological settings ([Garzanti et al.](#)  
233 [2018a](#)). Microcline with cross-hatch twinning is called for brevity “microcline” through the text.  
234 Median grain size was determined in thin section by ranking and visual comparison with standards  
235 of  $\phi/4$  classes prepared by sieving in our laboratory.

236 **Heavy minerals.** From a split aliquot of the widest convenient size-window obtained by wet  
237 sieving (mainly 15-500  $\mu\text{m}$ ), heavy minerals were separated by centrifuging in Na-polytungstate  
238 ( $2.90 \text{ g/cm}^3$ ) and recovered by partial freezing with liquid nitrogen. In grain mounts,  $\geq 200$  transparent  
239 heavy minerals for each sample were either grain-counted by the area method or point-counted at  
240 appropriate regular spacing to obtain correct volume percentages ([Garzanti and Andò 2019](#)).  
241 Mineralogical analyses were carried out by routinely coupling observations under the microscope and  
242 the Raman spectroscopy. Transparent heavy-mineral assemblages, called for brevity “tHM suites”  
243 throughout the text, are defined as the spectrum of detrital extrabasinal minerals with density  $>2.90$   
244  $\text{g/cm}^3$  identifiable under a transmitted-light microscope. According to the transparent-heavy-mineral  
245 concentration in the sample (tHMC), tHM suites are defined as extremely poor (tHMC  $< 0.1$ ), very

246 poor ( $0.1 \leq \text{tHMC} < 0.5$ ), poor ( $0.5 \leq \text{tHMC} < 1$ ), moderately poor ( $1 \leq \text{tHMC} < 2$ ), moderately rich  
 247 ( $2 \leq \text{tHMC} < 5$ ), rich ( $5 \leq \text{tHMC} < 10$ ), very rich ( $10 \leq \text{tHMC} < 20$ ), or extremely rich ( $\text{tHMC} > 20$ ).  
 248 The sum of zircon, tourmaline, and rutile over total transparent heavy minerals (**ZTR** index of [Hubert](#)  
 249 [1962](#)) expresses the chemical durability of the tHM suite. The “Amphibole Color Index” **ACI** varies  
 250 from 0 in detritus from greenschist, blueschist, or lowermost amphibolite-facies rocks yielding  
 251 exclusively blue or blue/green amphibole to 100 in detritus from granulite-facies or volcanic rocks  
 252 yielding exclusively brown amphibole ([Andò et al. 2014](#)).  
 253 Significant minerals are listed in order of abundance (high to low) throughout the text. Key  
 254 compositional parameters are summarized in [Table 1](#). The complete petrographic and heavy-mineral  
 255 datasets are provided in [Appendix Tables A2](#) and [A3](#).

256 **River morphometry.** The geomorphological properties of the Zambezi River and its major  
 257 tributaries were quantified using TopoToolbox, a set of MATLAB functions for the analysis of relief  
 258 and flow pathways in digital elevation models (DEM; [Schwanghart and Scherler 2014](#)). The analysis  
 259 of the longitudinal profile of bedrock channels was carried out on a 90 m-resolution DEM provided  
 260 by Shuttle Radar Topography Mission Global (SRTM GL3; <https://opentopography.org>) in order to  
 261 identify major knickpoints, defined as sites where the channel gradient changes abruptly owing to  
 262 sharp local changes in bedrock strength and/or uplift rate.

263 Channel concavity  $\theta$  and normalized channel-steepness  $k_{sn}$  (referenced to a fixed concavity 0.45 to  
 264 facilitate comparison among channel slopes with widely varying drainage areas and concavities) are  
 265 defined by the power-law relationship  $S = k_s A^{-\theta}$  between the local channel slope  $S$  and the  
 266 contributing drainage area  $A$  used as a proxy for discharge ([Flint 1974](#); [Whipple 2004](#)).

267

268

## Data

269

270 In the partitioned Zambezi sediment-routing system, sand compositional signatures are radically  
 271 different upstream and downstream of both Lake Kariba and Lake Cahora Bassa ([Table 1](#)), indicating

272 that no sand can pass across each reservoir. In the Uppermost Zambezi mainstem, as in some of its  
273 major tributaries including the Kwando and the Kafue, another factor hampering the continuity of  
274 downstream sediment transport is the occurrence of densely vegetated flat lowland occupied by  
275 numerous pans commonly aligned with shallow grassy valleys (*dambos*) acting as natural sediment  
276 traps (Moore et al. 2007).

277 ***The Uppermost Zambezi.*** Near the source, close to the political boundary between Zambia,  
278 Congo and Angola, sand is pure quartzose with K-feldspar >> plagioclase and a very poor tHM  
279 suite dominated by zircon with tourmaline, minor rutile, and staurolite (Fig. 4A). Kyanite increases  
280 downstream and clinopyroxene is significant upstream of the Kwando confluence.

281 The Kwando River from Angola contributes pure quartzose sand with a very poor tHM suite including  
282 zircon, tourmaline, kyanite, and staurolite (Fig. 5A). Sand of west-bank tributaries from Zambia  
283 ranges from quartz-rich feldspatho-quartzose with K-feldspar > plagioclase (Kabombo, Ngwezi) to  
284 pure quartzose with K-feldspar >> plagioclase (Kasaya). Muscovite occurs. The tHM suites vary from  
285 poor with tourmaline, rutile, epidote and kyanite (Kabombo) to very poor and including epidote,  
286 zircon, tourmaline, staurolite and green augite (Kasaya), or epidote-dominated with amphibole and  
287 minor garnet (Ngwezi).

288 ***The Upper Zambezi.*** Basaltic detritus from Karoo lavas mixes with quartz as the river approaches  
289 Victoria Falls, and in steadily increasing proportions across the gorges downstream of the falls.  
290 Upstream of Lake Kariba, bedload sand and levee silty sand include mafic volcanic rock fragments  
291 with lathwork and microlitic textures (Fig. 4B) and are, respectively, quartzose with plagioclase  $\approx$  K-  
292 feldspar and litho-feldspatho-quartzose with plagioclase >> K-feldspar. The moderately rich tHM  
293 suite consists almost entirely of green augite with a few olivine grains.

294 Upstream of Victoria Falls, the Sinda tributary from Zambia carries quartzose sand with mafic  
295 volcanic grains and a poor tHM suite dominated by brown and green augite. Basaltic detritus  
296 increases in tributary sand downstream of the falls. Masuie and Matetsi sands are, respectively, lithic-

297 rich litho-quartzose and quartzo-lithic basalticlastic, with rich and very rich tHM suites consisting  
 298 almost exclusively of augite and augite-bearing rock fragments.

299 River bars and levees of the Gwai River from Zimbabwe consist of feldspatho-quartzose sand with  
 300 plagioclase > K-feldspar (Fig. 5B). Mostly biotitic mica is concentrated in levee silty sand. The  
 301 moderately rich tHM suite consists of amphibole with subordinate epidote, garnet, and clinopyroxene.  
 302 The Deka River carries quartz-rich litho-quartzose basalticlastic sand with a very rich tHM suite  
 303 dominated by clinopyroxene with some epidote.

304 *The Middle Zambezi.* Downstream of Lake Kariba, Zambezi sand has the same feldspar-rich  
 305 feldspatho-quartzose composition as Kafue River sand, with K-feldspar >> plagioclase, some  
 306 metamorphic rock fragments, and micas (biotite  $\geq$  muscovite) (Figs. 4C and 5C). The rich tHM suite  
 307 includes amphibole (blue-green to green-brown hornblende and actinolite) and subordinate epidote,  
 308 kyanite, and clinopyroxene. Amphibole decreases and zircon increases slightly downstream the  
 309 mainstem.

310 The Luangwa River carries feldspatho-quartzose sand with K-feldspar >> plagioclase and granitoid  
 311 to gneissic rock fragments, with a moderately rich tHM suite including mainly amphibole (green-  
 312 brown to blue-green hornblende), kyanite, zircon, and prismatic or fibrolitic sillimanite (Fig. 5D).

313 *The Lower Zambezi.* In Mozambique, Zambezi sand ranges from quartzo-feldspathic to feldspar-  
 314 rich feldspatho-quartzose with K-feldspar  $\geq$  plagioclase (Fig. 4D). Mica (mostly biotite) is common  
 315 in very fine sand. The rich tHM suite includes mostly amphibole (blue-green to green-brown  
 316 hornblende and actinolite), subordinate epidote, locally strongly enriched garnet, and minor titanite,  
 317 zircon, clinopyroxene, and hypersthene.

318 Most tributaries contribute quartzo-feldspathic sand with K-feldspar  $\geq$  plagioclase and rich tHM suite  
 319 (Fig. 5E,F,G). An exception is represented by the Minjova and Zangue tributaries, which carry  
 320 feldspatho-quartzose and quartz-rich feldspatho-quartzose sand with poor tHM suite (Fig. 5H).  
 321 Feldspars (mostly plagioclase) are twice as abundant as quartz in Shire sand from Malawi. Metabasite

322 grains are significant in Morrunguze sand (Fig. 5E). Chacangara sand includes gabbroic, quartzose  
323 sandstone/metasediment, and shale/slate rock fragments.

324 The tHM suites are diverse. Amphibole (mainly green-brown and blue-green hornblende) is dominant  
325 in Mufa, Mazowe, Luenha, and Shire sand (ACI 31-50), and common in most other tributaries (ACI  
326 13-27 in Sangara, Chacangara, and Zangue sand but up to 80-91 in Sangadze and Minjova sand).  
327 Clinopyroxene and hypersthene are most abundant in Chacangara sand and also characterize Sangara,  
328 Morrunguze, Minjova and, to a lesser extent, Mufa sand (Table 1). Epidote is invariably present in  
329 moderate amounts. Garnet is dominant in Sangadze sand and common in Zangue and Minjova sand.  
330 Staurolite is associated with kyanite and prismatic or fibrolitic sillimanite in Zangue sand. Kyanite  
331 and sillimanite also occur in Luenha sand. Zircon and other durable minerals, as well as titanite and  
332 apatite, are minor (ZTR up to 8 in Sangara sand). Rare olivine was detected in Sangara, Chacangara,  
333 and Mufa sands.

334 *The northern coast, the shelf, and the slope.* Sand in the Bons Sinais estuary near Quelimane  
335 and adjacent beaches, located between 100 and 130 km north of the Zambezi mouth, is feldspatho-  
336 quartzose with plagioclase  $\geq$  K-feldspar and a rich tHM suite including mainly blue-green amphibole,  
337 subordinate epidote, clinopyroxene, and minor titanite, garnet, hypersthene, and mostly prismatic  
338 sillimanite (Fig. 4E).

339 Very fine-grained sand to coarse silt, cored on the upper continental slope ~85 km offshore of the  
340 Zambezi delta and close to the shelfbreak ~80 km to the ENE of the Bons Sinais mouth, is feldspar-  
341 rich feldspatho-quartzose with K-feldspar  $\approx$  plagioclase and a moderately rich tHM suite including  
342 blue-green amphibole, epidote, clinopyroxene, and minor prismatic sillimanite, titanite, tourmaline,  
343 apatite, hypersthene, and garnet. Benthic foraminifera are abundant (Fig. 4F). No major mineralogical  
344 difference is observed either between samples cored offshore of the Zambezi mouth and Quelimane  
345 area or among sediments deposited during the last glacial lowstand, the post-glacial sea-level  
346 transition, and the Holocene highstand in both areas.



## Sand generation in the Zambezi catchment

347  
348  
349  
350  
351  
352  
353  
354  
355  
356  
357  
358  
359  
360  
361  
362  
363  
364  
365  
366  
367  
368  
369  
370  
371  
372

*The Uppermost Zambezi: polycyclic sand from the Kalahari.* Sand generated in southeastern Angola and westernmost Zambia and carried by the Uppermost Zambezi and its Kwando tributary consists almost entirely of monocrystalline quartz with very poor, ZTR-dominated tHM suite including staurolite and kyanite, a mineralogical signature that reflects extensive recycling of Kalahari desert sand (Figs. 6 and 7). The sedimentary succession of this vast rim basin, formed on the low-relief southern Africa plateau confined between the rejuvenated shoulders of the Indian and Atlantic rifted margins, is largely of fluvial origin with secondary eolian imprint (Moore and Dingle 1998). Kalahari dunes are generally best developed west of river channels, suggesting deflation of fluvial sediments by easterly winds during drier periods (Shaw and Goudie 2002). Conversely, rivers have inundated interdune areas and incised their course across dune ridges during wetter periods (Thomas et al. 2000). Between a fourth and a half of quartz grains are well rounded in both dune and river sediments, indicating that climate-controlled cycling of quartz-rich sand has taken place repeatedly from the fluvial to the eolian environment and back (Thomas and Shaw 2002).

*The Upper Zambezi: mixing with detritus from Karoo basalts.* The Zambezi first meets Karoo basalt at Ngonye Falls in SW Zambia and from there on the river flows along Karoo rift basins as far as the Mozambican lowlands. Pure quartzose sand recycled from the Kalahari mixes downstream with detritus derived locally from Lower Jurassic Karoo basalt in increasing proportions, determined accurately with forward mixing models based on integrated petrographic and heavy-mineral data (Garzanti et al. 2012; Resentini et al. 2017).

Although the sand generation potential of basalt is notably less than that of sandstone or granite (Garzanti et al. 2019a, 2021a, 2021b; Le Pera and Morrone 2020; Morrone et al. 2020), mafic lava contains and sheds much more clinopyroxene than the few heavy minerals that quartzose sandstone contains and can thus supply. Therefore, wherever basaltic detritus mixes with recycled quartz, as in

373 the Upper Zambezi, quartz still dominates among main framework grains but the tHM suite rapidly  
374 becomes clinopyroxene-dominated (Figs. 6 and 7). From upstream of Victoria Falls to the Batoka  
375 Gorge, basaltic detritus accounts for < 3% of total sediment only and Upper Zambezi sand remains  
376 pure quartzose although clinopyroxene steadily increases from 14% to 86% of the very poor to poor  
377 tHM suite. Basaltic detritus increases to ~12% upstream of Lake Kariba, with composition changed  
378 to quartzose with 9% basaltic rocks fragments in bedload sand and to litho-feldspatho-quartzose in  
379 levee silty sand. Clinopyroxene represents 95% and 90% of the moderately rich and rich tHM suite,  
380 respectively.

381 Among Upper Zambezi tributaries, basaltic detritus represents ~10% of Sinde sand in Zambia, and  
382 ~15% of Shangani sand, 50% of Masuie sand, and up to 70% of Matetsi sand in Zimbabwe, the rest  
383 being mostly represented by quartz recycled from Kalahari dunes. Clinopyroxene invariably  
384 represents > 90% of the tHM suite in these rivers.

385 Such estimates are corroborated by clay-mineral and geochemical data, displaying an increase in  
386 smectite and in the concentration of Fe, Mg, Ca, Na, Sr, Ti, Eu, V, Cr, Mn, Co, Ni, Cu, and P along  
387 the Upper Zambezi, whereas the  $^{87}\text{Sr}/^{86}\text{Sr}$  and weathering indices decrease,  $\epsilon\text{Nd}_{(0)}$  becomes only  
388 moderately negative, and  $t_{\text{DM}}$  model ages younger (Garzanti et al. 2014a). Forward-mixing  
389 calculations based on the integrated geochemical dataset indicate that volcanic detritus increases from  
390 ~1% for sand and ~14% for cohesive (< 32  $\mu\text{m}$ ) mud upstream of Victoria Falls up to 17-18% for  
391 sand, 19-20% for sandy silt, and ~41% for cohesive mud upstream of Lake Kariba. These estimates  
392 imply that up to ~27% of the sand and ~45% of the mud that the Upper Zambezi carries towards Lake  
393 Kariba is generated downstream of Victoria Falls, from basaltic rocks of the Batoka Gorge and  
394 supplied by tributaries draining Karoo lavas and overlying Kalahari dunes.

395 ***The Middle Zambezi: first-cycle and recycled detritus from Zambia.*** The Middle Zambezi flows  
396 along Karoo extensional troughs (Fig. 2). These formed on top of the Kuunga suture zone, marking

397 the boundary between the Zimbabwe-Kalahari and Congo cratonic blocks and sealed during the final  
398 stages of the Neoproterozoic Pan-African orogeny (Goscombe et al. 2020).

399 The first major tributary joining the Zambezi ~70 km downstream of Lake Kariba is the Kafue River,  
400 which largely drains mid-Neoproterozoic volcano-sedimentary rocks and upper Tonian granites of  
401 the Lufilian Arc in the upper course. In the lowermost course, the Kafue cuts across the West Zambezi  
402 Belt, including polymetamorphic basement of the Congo Craton deformed at upper-amphibolite-  
403 facies conditions around 675 Ma (fig. 6 in Goscombe et al. 2020).

404 Because sand cannot pass Lake Kariba, Middle Zambezi sand downstream of the Kafue confluence  
405 acquires the same feldspar-rich feldspatho-quartzose metamorphiclastic signature of Kafue sand –  
406 with a little more siltstone/sandstone rock fragments and clinopyroxene derived locally from the  
407 Karoo Supergroup –, which is maintained as far as the confluence with the Luangwa River near the  
408 entry point into Lake Cahora Bassa (Fig. 8).

409 The Luangwa River, sourced in Paleoproterozoic gneisses of the Ubendian Belt, follows for most of  
410 its course another arm of the Karoo rift network. The Luangwa rift is bordered to the north by the  
411 external nappes of the Irumide Belt, including Paleoproterozoic granitoid gneiss overlain by quartzite  
412 and schist of the Muva Supergroup deformed at greenschist to amphibolite facies at 1.02-1.05 Ga (De  
413 Waele et al. 2009). Exposed to the south is the high-grade internal zone of the Southern Irumide  
414 Province (fig. 7 in Goscombe et al. 2020). Luangwa sand is thus a mixture of detritus derived from  
415 up to high-grade metamorphic rocks and recycled from Carboniferous to Jurassic siliciclastic strata,  
416 as indicated by relatively high quartz and ZTR minerals coexisting with blue-green to brown  
417 hornblende and mainly prismatic sillimanite.

418 ***The Lower Zambezi: feldspar-rich sand from Precambrian basements.*** As Upper Zambezi sand  
419 is dumped into Lake Kariba, Middle Zambezi sand is stored in Lake Cahora Bassa. Composition  
420 changes therefore again in the Lower Zambezi, where sand supplied by tributaries largely draining  
421 felsic to mafic igneous and up to high-grade metamorphic rocks acquires a quartzo-feldspathic

422 signature unique among the Earth's big rivers (Potter, 1978; Garzanti 2019). Most Lower Zambezi  
423 tributaries carry sand with Q/F ratio  $\leq 1$  (Fig. 6), reflecting mostly first-cycle provenance from mid-  
424 crustal crystalline basements. Detritus recycled from the sedimentary fill of Karoo, Cretaceous, or  
425 Cenozoic extensional basins is widespread, although subordinate. This is revealed by sandstone and  
426 shale rock fragments in Chacangara sand and by higher Q/F ratio and poor tHM suite in sand of the  
427 Zangue River draining the northern edge of the Urema Graben and of the Minjova River draining the  
428 Karoo Moatize-Minjova Basin (Fernandes et al. 2015).

429 The Sangara, Chacangara, and Mufa west-bank tributaries and the Morrunguze and Minjova east-  
430 bank tributaries drain high-grade rocks of the internal zone of the Southern Irumide Province  
431 including the Tete gabbro-anorthosite complex (fig. 1 in Goscombe et al. 2020). This is reflected by  
432 the occurrence of gabbroic or metabasite rock fragments and by up to very rich tHM suites including  
433 hypersthene and clinopyroxene, brown hornblende, and rare olivine.

434 The Luenha-Mazowe river system drains well into the Archean Zimbabwe Craton in the upper course  
435 and cuts downstream across the polymetamorphic Mudzi migmatitic gneisses remobilized during the  
436 Pan-African orogeny, and next across the Neoproterozoic Marginal Gneiss. The mostly first-cycle  
437 origin of their quartzo-feldspathic sand is reflected by the rich amphibole-dominated tHM suite, as in  
438 Mufa sand to the north (Fig. 7).

439 The lowest Q/F ratio is recorded in Shire sand, also including a very rich, amphibole-dominated tHM  
440 suite derived from granitic orthogneisses of the Blantyre domain (southern Malawi-Unango  
441 Complex), where Stenian-age crust underwent granulite-facies metamorphism during the Pan-  
442 African orogeny (Goscombe et al. 2020).

443 The Sangadze and Zangue lowermost-course tributaries are sourced in the Pan-African Umkondo  
444 Belt including greenschist-facies to lower-amphibolite-facies schists thrust onto the margin of the  
445 Zimbabwe Craton and upper amphibolite-facies migmatitic gneisses in the core, whereas the lower  
446 course cuts across the Cretaceous to Cenozoic sediment fill of the Lower Zambezi graben. Recycling

447 is manifested in Zangue sand by the highest Q/F ratio of all Lower Zambezi tributaries. Poor to  
448 moderately poor, garnet-dominated (Sangadze) or garnet-staurolite (Zangue) tHM suites reflect both  
449 first-cycle provenance from lower-amphibolite-facies metasediments of the Umkondo Belt and  
450 recycling of Cretaceous sandstones derived from them (e.g., Sena Formation; [Salman and Abdula](#)  
451 [1995](#)). The occurrence of brown amphibole and prismatic sillimanite, instead, reveals minor but  
452 significant contribution from upper amphibolite-facies to granulite-facies gneisses of the orogen's  
453 core (e.g., Stenian Barue complex; fig. 1 in [Goscombe et al. 2020](#)).

454 Forward mixing models based on integrated petrographic and heavy-mineral data suggest that most  
455 Lower Zambezi sand (60-80%) is generated in subequal proportions in the Luenha-Mazowe river  
456 system sourced in the Zimbabwe Craton and in the trunk-river catchment upstream of the Luenha  
457 confluence, including the Zambezi Belt and the Southern Irumide Province. Additional contributions  
458 from the Umkondo Belt and recycled from the Karoo, Cretaceous, or Cenozoic extensional basins  
459 drained by the Minjova, Sangadze, and Zangue tributaries are significant (~20%), whereas supply  
460 from the Tete gabbro-anortosite complex and Blantyre Domain, drained respectively by the  
461 Morrunguze and Shire tributaries, appears to be subordinate (~10%).

462 ***The Zambezi passive margin.*** Detrital modes of Lower Zambezi sand match neither those of  
463 estuary and beach sands in the northern delta near Quelimane nor sediments cored offshore of both  
464 the Zambezi mouth and Quelimane area and deposited during either the Holocene highstand or the  
465 previous post-glacial and glacial relative lowstands ([Table 1](#)). The Q/F ratio is  $1.0 \pm 0.1$  in Lower  
466 Zambezi sand but  $2.5 \pm 0.5$  in sand of the Quelimane area and  $1.6 \pm 0.3$  in offshore samples. The  
467 homogeneous composition of offshore sediments generated before the mid-Holocene (older than 4  
468 ka) suggests that this could represent the original, pre-Anthropocene signature of Zambezi sediment.  
469 Subsequent closure of the Kariba and Cahora Bassa dams – with consequent drastic reduction of the  
470 catchment area effectively contributing sediment to the Zambezi delta – explains the peculiar  
471 mineralogical signatures characterizing Lower Zambezi sand today. Besides the abundance of

472 feldspars, these include the high tHMC and ACI indices, reflecting provenance dominantly from  
473 middle crustal igneous and high-grade metamorphic rocks. The abundance of mica in offshore  
474 sediments, instead, is the effect of preferential winnowing of slow-settling platy phyllosilicates by  
475 waves, a phenomenon observed along continental shelves worldwide (e.g., [Doyle et al. 1968](#);  
476 [Garzanti et al. 2015, 2019b](#))

477 The mineralogy of estuary and beach sand in the Quelimane area is not the same as either Lower  
478 Zambezi or offshore sediment ([Table 1](#)). This is more difficult to explain, because predominantly  
479 northward littoral drift would be expected to entrain sand from the Zambezi delta, leading to  
480 homogeneous composition along the coast. Reasons of such discrepancy may include local reworking  
481 of floodplain sediments, whereas littoral drift from the north is unsupported by prevailing longshore-  
482 current patterns (fig. 4 in [Schulz et al. 2011](#); [van der Lubbe et al. 2014](#)).

483

#### 484 **How does Zambezi sand fit with classical sedimentary-petrology theories?**

485

486 The petrographic and mineralogical changes documented along the Zambezi sediment-routing system  
487 allow some considerations of consequence. In particular, they demonstrate how the knowledge  
488 acquired studying present landscapes argues against the uncritical use of simplistic concepts in  
489 geological research. In the lack of direct observations, we often try to unravel the past by using  
490 ungrounded simplifications and naïve analogies (e.g., sediment that “matures” in time like fruit),  
491 unable to constrain or even imagine the complexities of past sediment-routing systems including the  
492 effects of inheritance and multiple recycling. In the lack of clear evidence, we tend to implicitly  
493 assume that the information contained in the compositional signatures of sediments refers to the  
494 targeted sedimentary basin only, although it may — and commonly does — largely reflect tectonic  
495 or climatic conditions that existed, there or somewhere else, at earlier times. The present may well  
496 provide one key to the past, but how many are the doors and locks that this key is unable to open?  
497 *Are prêt-à-porter* models a help or a hindrance to the understanding of the complex 4D evolution of

498 geological entities through space and time? There are several specific questions that the present case  
499 study helps to investigate. The first one, tackled below, is: “*To what extent are classical provenance*  
500 *models adequate?*”

501 ***Provenance models.*** The first model linking sand mineralogy with the tectonic setting of source  
502 areas was developed by P.Krynine (1948), who inherited from his Moscow teacher M.S.Shvetsov  
503 (1934) the belief that sediment composition reflects systematic interactions among lithogenetic  
504 processes that can be unraveled and understood. The basic assumption is that the continental crust  
505 can be envisaged as consisting of sedimentary layers non-conformably overlying deformed  
506 metamorphic rocks intruded at depth by plutonic rocks. The progressive top-down erosion of such a  
507 rocky layer-cake would generate quartz-rich recycled sediments first, lithic-rich metamorphiclastic  
508 detritus next, and finally feldspar-rich plutoniclastic detritus. During a tectonically quiescent stage,  
509 recycling of cover strata would go on for a long time, eventually producing a wide sheet of quartzose  
510 sand (named “quartzite”). Conversely, tectonic uplift would lead to rapid unroofing of deep-seated  
511 plutonic rocks feeding fault-bounded basins with feldspar-rich sand (named “arkose”). These  
512 concepts were elaborated further by Krynine’s student at Pennsylvania State College R.L.Folk (1980  
513 p.108-144), who pointed out the insufficient attention dedicated by his teacher’s theory to sources of  
514 complexities such as geological inheritance, volcanism, and diversity of geodynamic settings.  
515 Furthermore, Folk acknowledged the major role of chemical weathering, and thus distinguished  
516 “*climatic arkose*”, generated from basement rocks in dry climate even during stages of tectonic  
517 quiescence, from Krynine’s “*tectonic arkose*”.

518 The essence of such lines of reasoning passed largely unaltered from the pre-plate-tectonic to the  
519 post-plate-tectonic era. The same three stages identified in Krynine’s and Folk’s models are  
520 recognized in W.R.Dickinson’s model (1985), where sediments produced in anorogenic (i.e.,  
521 subduction-unrelated) settings are designated as ***continental block*** provenance, distinguished into  
522 three subprovenances: *craton interior* (the quartz-rich sand produced during tectonically quiescent

523 stages), *transitional*, and *basement uplift* (the feldspar-rich sand shed from rapidly uplifted granitoid  
524 crustal blocks). Differently from Krynine's scheme, lithic-rich sediments were held to be diagnostic  
525 of orogenic (i.e., subduction-related) settings.

526 Heavy minerals were not organically considered in provenance models until later on (Nechaev and  
527 Isphording 1993; Garzanti and Andò 2007). One reason is that they are of limited use in ancient  
528 sediments wherever the tHM suite has been strongly depleted and modified by selective intrastratal  
529 dissolution of less durable species during diagenesis (Milliken 2007; Morton and Hallsworth 2007;  
530 Garzanti et al. 2018b). Moreover, the information carried by tHM suites may be profoundly distorted  
531 by hydrodynamic processes or fertility effects (Garzanti et al. 2009; Malusà et al. 2016). Heavy-  
532 mineral-rich sources such as mafic igneous and high-temperature or high-pressure metamorphic rocks  
533 have an overwhelming effect on the detrital tHM suite, heavy-mineral-poor sedimentary rocks or  
534 granite being conversely strongly under-represented (fig. 1 in Garzanti and Andò 2019). Because of  
535 the fertility effect, the tHM suite may reflect a radically different provenance than framework  
536 petrography, as in the Upper Zambezi where pure quartzose sand contains a clinopyroxene-dominated  
537 tHM suite.

538 Combining petrographic and heavy-mineral modes represents a necessary requirement to tackle the  
539 complexities of geological landscapes and achieve a refined provenance characterization. Anorogenic  
540 provenance could thus be subdivided into volcanic and non-volcanic and the latter, in turn, into  
541 *undissected* (craton interior), *transitional*, and *dissected* (basement uplift) continental block  
542 subprovenances (Garzanti et al. 2001). **Anorogenic volcanic** provenance is typified by feldspatho-  
543 lithic to quartzo-feldspatho-lithic sand with rich clinopyroxene-dominated tHM suite, undissected  
544 continental block subprovenance by quartzose sand with poor ZTR-dominated tHM suite, and  
545 dissected continental block subprovenance by quartzo-feldspathic sand with rich hornblende-  
546 dominated tHM suite (Garzanti 2016). Supply from continental flood basalts such as the Karoo  
547 (anorogenic volcanic provenance) is not contemplated in Dickinson's (1985) model. Consequently,



548 in a hypothetical analogous ancient case study, the uncritical use of that model would erroneously  
549 ascribe the compositional trend observed downstream the Upper Zambezi to mixing with arc-derived  
550 detritus.

551 Are models right or wrong? Obviously neither. As any tool, they apply well to some circumstances  
552 and badly to others. Because they are derived from one setting and extrapolated to another, and  
553 because different settings are not the same by definition, models are bound to be partly misleading  
554 even in the luckiest case ([Garzanti and Sternai 2020](#)). Their uncritical use is therefore discouraged.

555 *The final signature of Zambezi sand.* The Zambezi River carries to the Indian Ocean quartzo-  
556 feldspathic sand, a fingerprint that has hardly an equivalent among the world's big rivers ([Potter 1978](#);  
557 [Garzanti 2019](#)). Such a composition compares with that of granitoid-derived sand generated in dry  
558 southern California (table 3 in [Dickinson 1985](#)) and represents a typical mark of *dissected continental*  
559 *block* subprovenance. Shire sand is the richest in feldspars and thus a good example of “*ideal arkose*”  
560 ([Dickinson 1985](#)).

561 Vast river catchments typically embrace a very wide range of rocks produced in different geodynamic  
562 settings at different times. Their sediments are thus mixtures of different provenances including a  
563 considerable fraction of recycled grains. Lower Zambezi sand — characterized by feldspar  $\approx$  quartz,  
564 very few aphanite lithics, and a rich hornblende-dominated tHM suite largely shed first-cycle from  
565 plutonic and high-grade metamorphic rocks — represents an anomaly in this respect. One main  
566 reason, discussed further below, is that quartz-dominated sand recycled in the upper reaches is not  
567 transferred to the lower course. Detritus reaching the Indian Ocean is thus generated mostly in eastern  
568 Zimbabwe, central Mozambique, and southern Malawi, where the roots of Archean cratons and  
569 Proterozoic orogens have been uplifted and progressively eroded during the southward propagation  
570 of the East African rift ([Fernandes et al. 2015](#)). Consequently, sand composition is the same as detritus  
571 shed from mid-crustal basement rocks exposed along actively uplifted and deeply dissected rift

572 shoulders, such as those flanking the Red Sea ([Garzanti et al. 2001, 2013a](#)), rather than that expected  
573 for a mature passive margin.

574 *Do minerals “mature” during fluvial transport?* A widely held belief in sedimentary petrology  
575 – persistent although long demonstrated untrue (e.g., [Russell 1937](#); [Shukri 1950](#)) – is that chemically  
576 and mechanically durable minerals must increase at the expense of unstable and less resistant minerals  
577 during long-distance fluvial transport.

578 Uppermost Zambezi sand consists almost entirely of quartz associated with the most durable heavy  
579 minerals zircon, tourmaline and rutile, thus representing a good example of “highly mature” sediment  
580 ([Folk 1951](#); [Hubert 1962](#)). In the Upper Zambezi downstream, however, mafic volcanic rock  
581 fragments increase and clinopyroxene becomes first a significant, then the main, and finally the nearly  
582 exclusive transparent heavy mineral. The progressive downstream increase of detritus derived from  
583 Karoo lavas, locally including unstable olivine, results in decreasing degree of “maturation”  
584 downstream. Decreasing “maturity” with transport distance – which sounds paradoxical because  
585 maturation is by definition intended to progress irreversibly with the passing of time — is not unusual  
586 in modern rivers wherever less durable detrital components are added downstream, as observed for  
587 instance along the Kagera River in equatorial Africa ([Garzanti et al. 2013b](#)).

588 In the Middle Zambezi, sand is notably enriched in feldspars and diverse types of rock fragments  
589 supplied by the Kafue and other tributaries draining both Precambrian orogenic belts and Permo-  
590 Triassic rift-basin fills. Composition thus becomes even less “mature”. In the Lower Zambezi, owing  
591 to prominent supply from local tributaries draining mid-crustal Precambrian basements, quartz  
592 content decreases further, becoming equally or even less abundant than feldspar.

593 The Zambezi is thus an exemplary case of sediment-routing system along which the ratio between  
594 stable and unstable minerals (too often inappropriately portrayed as degree of “maturity”; [Garzanti](#)  
595 [2017](#)) decreases steadily with distance. Although enhanced by the artificial segmentation of the river  
596 course after the closure of Kariba and Cahora Bassa dams, preventing the continuity of sand transport

597 across the reservoirs, such a trend towards less durable mineralogical assemblages downstream is  
598 primarily a natural phenomenon reflecting the multistep evolution of the river and location of  
599 erosional foci (Fig. 9).

600 The Zambezi progressively connected stepwise the broad low-relief southern Africa plateau underlain  
601 by thick cratonic crust and sustained by dynamic uplift since mid-Cenozoic times (Lithgow-Bertelloni  
602 and Silver 1998; Moore et al. 2009b; Flügel et al. 2018) with the middle and lower reaches, entrenched  
603 in Karoo rifts and cutting across Precambrian mobile belts rejuvenated by the southward propagation  
604 of the East African rift in the late Neogene (Roberts et al. 2012; Hopper et al. 2020). If we just looked  
605 at the compositional signature of Lower Zambezi sand and uncritically applied traditional ideas of  
606 “maturity” disregarding the character and history of the catchment, then we would falsely infer a  
607 scenario similar to Red Sea shoulders, involving short fluvial transport from locally uplifted rift  
608 highlands. The largest river sourced in the heart of cratonic southern Africa would be left unseen.

609 ***Broken transmission of provenance signals: the anthropogenic effect.*** One main reason why  
610 traditional petrological models apply so badly to the Zambezi is the pronounced segmentation of the  
611 fluvial system, which reflects its multistep Neogene evolution finally fixed by man’s construction of  
612 Kariba and Cahora Bassa dams. Development of the Zambezi River is held to have started by  
613 headward erosion operated by a coastal river that captured first the Luangwa and next the Kafue  
614 Rivers after re-incision of the Cahora Bassa and Gwembe troughs upstream. Only sometime around  
615 the early Pleistocene was the gentle-gradient Upper Zambezi captured as well, finally linking the  
616 Kalahari Plateau with the Indian Ocean *via* Victoria Falls (Moore et al. 2007).

617 Rim basins such as the Mega-Kalahari represent huge reservoirs of quartz-rich polycyclic sand stored  
618 in continental interiors. Such reservoirs may be tapped by headward-eroding coastal rivers that  
619 progressively enhance their discharge as larger segments of endorheic drainage are captured, a  
620 process continuing today with incipient piracy of the Okavango (Moore and Larkin 2001).

621 The *undissected continental block* (craton interior) subprovenance signal carried by the Upper  
622 Zambezi, however, fails to be transmitted beyond Lake Kariba. In the same way, the *transitional*  
623 *continental block* subprovenance signal carried by the Middle Zambezi fails to be transmitted  
624 downstream of Lake Cahora Bassa. The Lower Zambezi thus carries a pure *dissected continental*  
625 *block* (basement uplift) subprovenance signal to the Indian Ocean, the same that the coastal proto-  
626 Zambezi would have had before starting its inland expansion punctuated by the progressive capture  
627 of interior drainage.

628 River segmentation was far less pronounced before man's intervention, as indicated by the poor  
629 compositional match between the present Lower Zambezi sand and upper Quaternary offshore  
630 sediments, which have notably higher Q/F ratio and a little more clinopyroxene. Such differences  
631 cannot be dismissed as a grain-size effect, because the Q/F ratio typically increases with increasing  
632 grain size (e.g., [Garzanti et al. 2021c](#)) and our river samples are very fine to fine sands whereas  
633 offshore samples are sandy silts. Rather than additional contribution by longshore-drifting sediment  
634 from outside the Zambezi delta, the plausible explanation is that a larger amount of detritus generated  
635 in the upper and middle catchment reached the ocean before closure of Kariba and Cahora Bassa  
636 dams. Forward-mixing calculations allow us to estimate that, before the Anthropocene, as much as  
637 40% of detritus transferred to the coast was generated by erosion of Phanerozoic covers (~35%  
638 recycled from pure quartzose sand or sandstone and ~5% from basalt). Quartz-rich sand and  
639 sandstones and Karoo lavas are widespread in the Zambezi catchment, from Ngonye Falls in the  
640 Uppermost Zambezi to the lowermost course. The pre-Anthropocene contributions from the Upper  
641 or Middle Zambezi are therefore hard to accurately quantify, although the sharp mineralogical  
642 contrast between Upper Zambezi and offshore sediments indicates that most detritus was derived from  
643 the middle-lower reaches even in pre-Anthropocene times ([Fig. 9A,B,C](#)).

644 ***Weathering effects inherited from the past.*** The last question dealt with here concerns the  
645 possibility to infer climate from mineralogical composition of sand. Spurred by optimism, researchers

646 have widely used chemical indices (e.g.,  $CIA = [Al_2O_3 / (Al_2O_3 + K_2O + Na_2O + CaO^*)] \cdot 100$ ; Nesbitt  
647 and Young 1982) or even mineralogical indices (e.g.,  $MIA = Q / (Q + F) \cdot 100$ ; Rieu et al. 2007) to infer  
648 climatic conditions in strata as old as the Paleoproterozoic. Studies of modern sedimentary systems,  
649 however, recommend caution (Garzanti and Resentini 2016). If we interpret compositional data  
650 uncritically using simplistic concepts, then we are bound to make severe mistakes.

651 Because feldspars are scarce in the Uppermost Zambezi ( $Q / (Q + F) \geq 95\%$ ) and abundant in the Lower  
652 Zambezi ( $Q / (Q + F) \approx 50\%$ ), an inconsiderate use of the MIA would suggest very humid climate in  
653 the Kalahari and very dry climate in Mozambique. Which is patently wrong. Beside being subject to  
654 marked grain-size control (Garzanti et al. 2021c and references therein), the  $Q / (Q + F)$  ratio reaches  
655 100% in sand of both hyper-humid equatorial Congo and hyper-arid tropical Arabian or Sahara sand  
656 seas (Garzanti et al. 2013a, 2019c; Pastore et al. 2021), making it evident that climatic conditions  
657 cannot be naïvely inferred by mineralogical parameters such as the MIA.

658 The Uppermost Zambezi and its Kwando tributary carry pure quartzose sand mostly recycled from  
659 eolian dunes that grew across the Mega-Kalahari Desert during arid stages of the Quaternary (Thomas  
660 and Shaw 2002). In a desert climate, generation of pure quartzose sand cannot occur in a single  
661 sedimentary cycle, but requires widespread recycling of older sandstones affected by extensive  
662 chemical weathering in very different climatic conditions. Pure quartzose composition of sand, as  
663 well as abundant kaolinite in mud (Garzanti et al. 2014a), thus represent the echo of a time when  
664 sediments were produced in a chemically aggressive hot-humid climate.

665 In heavy-mineral suites of Uppermost Zambezi and Kwando sands, this is reflected by the scarcity of  
666 garnet relative to staurolite, kyanite, andalusite, and sillimanite [ $Grt / (Grt + SKA) < 5\%$ ]. These  
667 minerals characterize amphibolite-facies metasedimentary rocks and unweathered detritus derived  
668 from them, where garnet is almost invariably dominant [ $Grt / (Grt + SKA) = 70 \pm 20\%$ ; Garzanti et al.  
669 2006, 2010]. This is the case for sand of the Lower Zambezi and its major tributaries (Fig. 7 middle  
670 panel). In the Upper Zambezi, instead, staurolite and kyanite are common but garnet very scarce,

671 which cannot be explained by either provenance or hydraulic factors (garnet being only slightly  
672 denser) and is most plausibly ascribed to the low stability of garnet in a humid subequatorial climate  
673 (Garzanti et al. 2013b). Dominance of quartz, abundance of kaolinite, and scarcity of garnet in Upper  
674 Zambezi sediment as well as in Kalahari dunes (Garzanti et al. 2014a, 2014b) thus consistently reflect  
675 humid subequatorial conditions that reigned in the past, dating back to the Cenozoic or Mesozoic well  
676 before the arid Quaternary when Kalahari dunes invaded the landscape (Guillocheau et al. 2015,  
677 2018).

678 Today, climate is arid enough to induce only limited weathering in most of southern Africa, where  
679 detrital modes largely reflect the dominant parent lithologies exposed in source areas. In  
680 Mozambique, where climate ranges from hot semiarid in the interior to tropical savanna downstream  
681 the Zambezi Valley (*Bsh* to *Aw* classes of the Köppen climate classification), feldspars are more  
682 abundant than in any other big river on Earth. Olivine, which is considered to be a most unstable  
683 detrital mineral, occurs in small amounts both in the mainstem upstream of Lake Kariba and in  
684 western tributaries joining the Zambezi shortly downstream of Cahora Bassa. Sand mineralogy thus  
685 fails to reflect a notable effect of weathering occurring at present across most of the Zambezi  
686 catchment.

687

688

## 688 Conclusions

689

690 Sand in the Uppermost Zambezi is pure quartzose and almost entirely recycled from desert dunes  
691 across the Kalahari Plateau, thus matching the theoretical sediment composition produced in cratonic  
692 interiors (*undissected continental block* subprovenance). At the opposite end of both the drainage  
693 basin and the petrologic spectrum of sediment shed from continental blocks, sand of the Lower  
694 Zambezi and many of its major tributaries is quartzo-feldspathic, even reaching an “ideal arkose”  
695 composition (*dissected continental block* subprovenance). Sand of the Middle Zambezi and its major  
696 tributaries has an intermediate feldspatho-quartzose composition (*transitional continental block*

697 subprovenance). The relative abundance of durable quartz and ZTR minerals thus decreases steadily  
698 along the sediment-routing system, a trend that denies the naïve but still popular idea that sediment  
699 “matures” with transport distance.

700 Although enhanced by the artificial segmentation of the river course after the closure of the Kariba  
701 and Cahora Bassa dams that prevented the continuity of sand transport across the reservoirs, such a  
702 downstream trend towards less durable mineralogical assemblages is primarily a natural phenomenon  
703 reflecting the dynamic uplift of the low-relief plateau of cratonic central southern Africa in the upper  
704 reaches and polyphase, ongoing rift-related rejuvenation of Precambrian mobile belts in the middle  
705 and lower reaches.

706 The thorough investigation of each part of the river catchment and the precise definition of the  
707 mineralogical correspondence between parent rocks and daughter sediments is indispensable to forge  
708 a key able to unlock the sedimentary archives represented by the thick stratigraphic successions  
709 accumulated throughout the late Mesozoic and Cenozoic in onshore and offshore basins, and thus  
710 reconstruct with improved robustness the complex history of the Zambezi River.

711

712

713

## ACKNOWLEDGMENTS

714

715 The article benefited from careful reviews by Matthias Hinderer and Emilia Le Pera. We are very  
716 grateful to Sonwabile Kidwell Rasmeni and Baojin Zhao for their fundamental contribution to the  
717 sampling campaign, and to captains, crew, and scientists of the PAMELA-MOZ04 survey onboard  
718 the R/V *Pourquoi pas?* which allowed us to collect the offshore samples. The oceanographic  
719 PAMELA-MOZ04 cruise was part of the PAMELA (Passive Margin Exploration Laboratories)  
720 scientific project led by IFREMER and TOTAL in collaboration with the Université de Bretagne  
721 Occidentale, Université Rennes 1, Université Pierre and Marie Curie, CNRS, and IFPEN. Estuary

722 and beach samples from the Quelimane area were kindly provided by Celso de Carvalho Matsinhe  
723 (Tongji Univeristy, Shanghai). Funding was contributed by the National Research Foundation of  
724 South Africa (NRF), Water Research Commission of South Africa (WRC), African Institute of  
725 Mathematical Sciences (AIMS), and Project MIUR – Dipartimenti di Eccellenza 2018–2022,  
726 Department of Earth and Environmental Sciences, University of Milano-Bicocca.

727

728

### SUPPLEMENTARY MATERIAL

729

730 Supplementary data associated with this article, to be found in the online version at  
731 [http://dx.doi.\\_\\_\\_\\_\\_](http://dx.doi._____), include information on sampling sites (Table A1) together with the  
732 complete bulk-sand petrography (Table A2) and heavy-mineral datasets (Table A3). The Google-  
733 Earth® map of sampling sites [Zambezi.kmz](#) is also provided.

734

735

### DATA AVAILABILITY

736

737 Sediment cores collected offshore Mozambique are curated at IFREMER core repository in Plouzané  
738 (France). Core data related to this article can be requested at:

739 Core MOZ4-CS14: IGSN BFBGX-85862 (<http://igsn.org/BFBGX-85862>)

740 Core MOZ4-CS17: IGSN BFBGX-85865 (<http://igsn.org/BFBGX-85865>)



## FIGURE CAPTIONS

741

742

743 **Figure 1.** The Zambezi drainage basin (base map from Google Earth®). White circles indicate  
744 sampling locations (more information in file [Zambezi.kmz](#)). VF = Victoria falls.

745 **Figure 2.** Geological domains in the Zambezi catchment and adjacent regions (after [Hanson 2003](#)  
746 and [CGMW-BRGM 2016](#)). CK = Choma-Kalomo block; IB = Irumide Belt; KB = Kibaran Belt; LRZ  
747 = Luangwa Rift Zone, activated in the Permian and reactivated in the Neogene; MB = Magondi Belt;  
748 MRZ = Malawi Rift Zone; SIB = South Irumide Belt, deeply affected by the Pan-African orogeny;  
749 UB = Umkondo Belt; Ub-Usg = Ubendian-Usagaran Belts.

750 **Figure 3.** River morphometry (same vertical scale for all profiles; same horizontal scale for  
751 tributaries). Besides the concave equilibrium profile of the Kwando, longitudinal channels are highly  
752 irregular, as highlighted by extreme variations in both steepness and concavity indices  $k_{sn}$  and  $\theta$ . As  
753 most rivers in southern Africa, the Zambezi and several tributaries (e.g., Gwai, Kafue, Shire) display  
754 youthful, staircase profiles with long flat segments separated by very steep tracts, reflecting the  
755 presence of stepped planation surfaces separated by escarpments, a characteristic feature of southern  
756 African landscape ([Knight and Grab 2018](#)).

757 **Figure 4.** Petrographic changes along the Zambezi sediment-routing system from source to sink. **A)**  
758 Pure quartzose sand recycled from the Mega-Kalahari Desert. **B)** Marked enrichment in lathwork to  
759 microlitic volcanic rock fragments and clinopyroxene in quartzose sand downstream of Victoria Falls.  
760 **C)** Reconstituted feldspatho-quartzose metamorphiclastic bedload downstream of Lake Kariba. **D)**  
761 Sharp increase in feldspars in reconstituted bedload downstream of Lake Cahora Bassa. **E)**  
762 Feldspatho-quartzose beach sand in the Quelimane area. **F)** Very fine-grained feldspar-rich  
763 feldspatho-quartzose sand containing benthic foraminifera (stained by alizarine red) and deposited  
764 during the last glacial lowstand on the upper slope offshore of the Zambezi mouth. All photos with  
765 crossed polars; blue bar for scale = 100  $\mu\text{m}$ .

766 **Figure 5.** Sand composition in major Zambezi tributaries. **A)** Up to well rounded monocrystalline  
 767 quartz grains recycled from Mega-Kalahari dunes. **B)** High-rank metamorphic rock fragments and  
 768 microcline derived first-cycle from the Magondi Belt. **C)** Biotite-rich metamorphic detritus from the  
 769 Lufilian Arc and Zambezi Belt mixed with rounded recycled quartz. **D)** Deeply corroded quartz and  
 770 feldspar grains derived from the Irumide Belt and recycled from Karoo strata. **E)** Abundant  
 771 microcline with high-rank metamorphic rock fragments from the Archean Zimbabwe Craton and  
 772 Proterozoic gneisses. **F)** Microcline, gabbroic rock fragments, pyroxene, and amphibole from the  
 773 southern Irumide Belt and Tete gabbro-anortosite complex. **G)** Dominant feldspar derived from  
 774 orthogneisses and granulites of the Blantyre domain. **H)** Skeletal quartz and weathered K-feldspar  
 775 grains in Mozambican lowlands. All photos with crossed polars; blue bar for scale = 100  $\mu\text{m}$ .

776 **Figure 6.** Downstream quartz decrease along the segmented Zambezi sediment-routing system.  
 777 Composition changes stepwise from pure quartzose (Uppermost Zambezi) to quartzose volcaniclastic  
 778 (Upper Zambezi), feldspar-rich feldspatho-quartzose (Middle Zambezi), and finally quartzo-  
 779 feldspathic metamorphiclastic (Lower Zambezi). Symbol size is roughly proportional to tributary size  
 780 and increases downstream along the mainstem. Smaller symbols with thicker outline are Upper  
 781 Zambezi and Gwai River levee samples representing deep suspended load. Q = quartz; F = feldspars  
 782 (P = plagioclase; K = K-feldspar); L= lithics (Lm = metamorphic; Lv = volcanic; Ls = sedimentary).  
 783 Fields in the QFL diagram after [Garzanti \(2019\)](#); in the nested blue version of the same QFL plot,  
 784 data are centered to allow better visualization of quartz-rich samples ([von Eynatten et al. 2002](#)).

785 **Figure 7.** Changes in transparent-heavy-mineral suites downstream the segmented Zambezi  
 786 sediment-routing system. Note: 1) dominance of durable ZTR (zircon, tourmaline and rutile) and  
 787 SKA minerals (staurolite, kyanite, sillimanite, and andalusite) in the Uppermost Zambezi; 2)  
 788 progressive increase in clinopyroxene along the Upper Zambezi; 3) sharp increase in basement-  
 789 derived garnet (Grt), amphibole (Amp) and epidote (Ep) in the Middle and Lower Zambezi. Scarcity  
 790 of garnet in Uppermost and Upper Zambezi sand is ascribed to high weatherability inherited from

791 past hot-humid subequatorial climate. Symbol size is roughly proportional to tributary size and  
 792 increases downstream along the mainstem. Smaller symbols with thicker outline are Upper Zambezi  
 793 and Gwai River levee samples representing deep suspended load.

794 **Figure 8.** Stepwise changes in compositional signatures along the segmented Zambezi sediment-  
 795 routing system. Pure quartzose sand in the Uppermost Zambezi and Kwando Rivers is progressively  
 796 enriched in clinopyroxene and basaltic rock fragments downstream the Upper Zambezi. Middle  
 797 Zambezi sand chiefly reflects contribution from the Kafue River. Lower Zambezi sand is markedly  
 798 enriched in feldspars, amphibole, and garnet largely derived from Irumide Belts strongly affected by  
 799 the Pan-African orogeny. The biplot ([Gabriel 1971](#)) displays multivariate observations (points) and  
 800 variables (rays). The length of each ray is proportional to the variance of the corresponding variable;  
 801 if the angle between two rays is  $0^\circ$ ,  $90^\circ$ , or  $180^\circ$ , then the corresponding variables are perfectly  
 802 correlated, uncorrelated, or anticorrelated, respectively. Symbols as in [Figs. 6 and 7](#).

803 **Figure 9.** Zambezi river sands compared to coastal and offshore sediments. **A, B, C)** Uppermost and  
 804 Upper Zambezi detritus is clearly distinct from any downstream sample. Sediment fed into the Indian  
 805 Ocean was thus mostly derived from the middle-lower catchment even before closure of the Kariba  
 806 and Cahora Bassa dams. **D)** Passive margin sediments, however, do not closely match either Middle  
 807 or Lower Zambezi sand, suggesting significant additional contribution from both the upper catchment  
 808 and Mozambican lowlands in pre-Anthropocene times. Biplots **C** and **D** ([Gabriel 1971](#)) drawn with  
 809 *CoDaPack* software by [Comas-Cufí and Thió-Henestrosa \(2011\)](#). Q = quartz; P = plagioclase; K =  
 810 K-feldspar; ZTR = zircon + tourmaline + rutile; Cpx = clinopyroxene; Ep = epidote; Sil = sillimanite.

811 **Table 1.** Key petrographic and heavy-mineral signatures. Q = quartz; F = feldspars (P = plagioclase);  
 812 L = lithic grains (Lvm = volcanic to low-rank metavolcanic; Lsm = sedimentary to low-rank  
 813 metasedimentary; Lmfb = high-rank felsic metamorphic and metabasite); tHMC = transparent heavy-  
 814 mineral concentration; ZTR = zircon + tourmaline + rutile; Ap = apatite; Ttn = titanite; Ep = epidote;

815 Grt = garnet; St = staurolite; Ky = kyanite; Sil = sillimanite; Amp = amphibole; Cpx = clinopyroxene;  
816 Hy = hypersthene; &tHM = other transparent heavy minerals (mainly anatase and andalusite with  
817 locally monazite, olivine, or enstatite); ACI = Amphibole Color Index; n.d. = not determined. VF =  
818 Victoria Falls.  
819

## REFERENCES CITED

- 820  
821
- 822 Andò, S., Morton, A., and Garzanti, E., 2014. Metamorphic grade of source rocks revealed by  
823 chemical fingerprints of detrital amphibole and garnet. Geological Society, London, Special  
824 Publications 386:351-371.
- 825 Banks, N.L., Bardwell, K.A., and Musiwa S., 1995. Karoo Rift basins of the Luangwa Valley,  
826 Zambia. In: Lambiase, J.J. (ed.), Hydrocarbon Habitat in Rift Basins. Geological Society  
827 London, Special Publication 80:285-295.
- 828 Beiersdorf, H., Kudrass, H.R., and von Stackelberg, U., 1980. Placer deposits of ilmenite and zircon  
829 on the Zambezi Shelf. Geologisches Geol. Jahrbuch D36:5–85.
- 830 Bicca, M.M., Philipp, R.P., Jelinek, A.R., Ketzer, J.M.M., dos Santos Scherer, C.M., Jamal, D.L. and  
831 dos Reis, A.D., 2017. Permian-Early Triassic tectonics and stratigraphy of the Karoo Supergroup  
832 in northwestern Mozambique. Journal of African Earth Sciences 130:8-27.
- 833 Boniface, N., and Appel, P., 2018. Neoproterozoic reworking of the Ubendian Belt crust: Implication  
834 for an orogenic cycle between the Tanzania Craton and Bangweulu Block during the assembly  
835 of Gondwana. Precambrian Research 305:358-385.
- 836 Catuneanu, O., Wopfner, H., Eriksson, P.G., Cairncross, B., Rubidge, B.S., Smith, R.M.H., and  
837 Hancox, P.J., 2005. The Karoo basins of south-central Africa. Journal of African Earth Sciences  
838 43(1-3):211-253.
- 839 CGMW-BRGM, 2016. In: Thiéblemont, D. (Ed.), Geological Map of Africa, 1:10 Million Scale,  
840 [www.brgm.fr](http://www.brgm.fr).
- 841 Collins, A.S., Reddy, S.M., Buchan, C., and Mruma, A., 2004. Temporal constraints on  
842 Palaeoproterozoic eclogite formation and exhumation (Usagaran Orogen, Tanzania). Earth and  
843 Planetary Science Letters 224(1-2):175-192.
- 844 Comas-Cufí, M., and Thió-Henestrosa, F.S., 2011. CoDaPack 2.0: A Stand-Alone, Multi-Platform  
845 Compositional Software
- 846 Cox, K. G. 1989. The role of mantle plumes in the development of continental drainage patterns.  
847 Nature 342:873–877.
- 848 De Waele, B., Kampunzu, A.B., Mapani, B.S.E., and Tembo, F., 2006. The Mesoproterozoic Irumide  
849 belt of Zambia. Journal of African Earth Sciences 46(1-2):36-70.

- 850 De Waele, B., Fitzsimons, I.C.W., Wingate, M.T.D., Tembo, F., Mapani, B., and Belousova, E.A.,  
851 2009. The geochronological framework of the Irumide Belt: a prolonged crustal history along  
852 the margin of the Bangweulu Craton. *American Journal of Science* 309(2):132-187.
- 853 Debruyne, D., Hulsbosch, N., Van Wilderode, J., Balcaen, L., Vanhaecke, F., and Muchez, P., 2015.  
854 Regional geodynamic context for the Mesoproterozoic Kibara Belt (KIB) and the Karagwe-  
855 Ankole Belt: Evidence from geochemistry and isotopes in the KIB. *Precambrian Research* 264:  
856 82-97.
- 857 Derricourt, R.M., 1976, Regression rate of the Victoria Falls and the Batoka Gorge. *Nature* 264:23-  
858 25.
- 859 Dickinson, W.R., 1985. Interpreting provenance relations from detrital modes of sandstones. In:  
860 Zuffa, G.G. (Ed.), *Provenance of Arenites*. Reidel, Dordrecht, NATO ASI Series 148:333–361.
- 861 Doyle, L.J., Cleary, W.J., and Pilkey, O.H., 1968. Mica: its use in determining shelf-depositional  
862 regimes. *Marine Geology* 6:381-389.
- 863 Droz, L., and Mougénot, D., 1987. Mozambique upper fan: Origin of depositional units. *American*  
864 *Association of Petroleum Geologists Bulletin* 71(11):1355-1365.
- 865 Ebinger, C.E., and Scholz, C. A. 2012. Continental rift basins: The East African perspective. In:  
866 Busby, C., Azor, A. (eds.), *Tectonics of sedimentary basins: recent advances*. Oxford, Wiley-  
867 Blackwell, pp.185–208.
- 868 Eglinger, A., Vanderhaeghe, O., André-Mayer, A.S., Goncalves, P., Zeh, A., Durand, C., and Deloule,  
869 E., 2016. Tectono-metamorphic evolution of the internal zone of the Pan-African Lufilian  
870 orogenic belt (Zambia): Implications for crustal reworking and syn-orogenic uranium  
871 mineralizations. *Lithos* 240:67-188.
- 872 Fernandes, P., Cogné, N., Chew, D.M., Rodrigues, B., Jorge, R.C.G.S., Marques, J., Jamal, D., and  
873 Vasconcelos, L., 2015. The thermal history of the Karoo Moatize-Minjova Basin, Tete Province,  
874 Mozambique: An integrated vitrinite reflectance and apatite fission track thermochronology  
875 study. *Journal of African Earth Sciences* 112:55-72.
- 876 Fierens, R., Droz, L., Toucanne, S., Raïsson, F., Jouet, G., and Babonneau, N., 2019. Late Quaternary  
877 geomorphology and sedimentary processes in the Zambezi turbidite system (Mozambique  
878 Channel). *Geomorphology* 334:1–28.
- 879 Fierens, R., Toucanne, T., Droz, L., Jouet, G., Raïsson, F., Jorissen, E.L., Bayon, G., Giraudeau, J.,  
880 and Jorry, S.J., 2020. Quaternary sediment dispersal in the Zambezi turbidite system (SW Indian

- 881 Ocean). *Marine Geology* 428:106276, doi:[10.1016/j.margeo.2020.106276](https://doi.org/10.1016/j.margeo.2020.106276).
- 882 Flint, J.J., 1974. Stream gradient as a function of order, magnitude, and discharge. *Water Resources*  
883 *Research* 10:969–973.
- 884 Flügel, T.J., Eckardt, F.D., and Cotterill, W.P.D., 2018. The geomorphology and river longitudinal  
885 profiles of the Congo-Kalahari Watershed. In Runge, J. (ed.), *The African Neogene-Climate,*  
886 *Environments and People: Palaeoecology of Africa*. CRC Press, Leiden, The Netherlands 34:31-  
887 52.
- 888 Folk, R.L., 1951, Stages of textural maturity in sedimentary rocks. *Journal of Sedimentary Petrology*  
889 21:127–130.
- 890 Folk, R.L., 1980. *Petrology of Sedimentary Rocks*. Hemphill Publishing Co., Austin (USA), pp. 184.
- 891 Frimmel, H.E., Basei, M.S., and Gaucher, C. 2011, Neoproterozoic geodynamic evolution of SW-  
892 Gondwana: a southern African perspective. *Int. J. Earth Sci.* 100:323-354.
- 893 Fritz, H., Abdelsalam, M., Ali, K.A., Bingen, B., Collins, A.S., Fowler, A.R., Ghebreab, W.,  
894 Hauzenberger, C.A., Johnson, P.R., Kusky, T.M., and Macey, P., 2013. Orogen styles in the East  
895 African Orogen: a review of the Neoproterozoic to Cambrian tectonic evolution. *Journal of*  
896 *African Earth Sciences* 86:65-106.
- 897 Gabriel, K.R., 1971. The biplot graphic display of matrices with application to principal component  
898 analysis. *Biometrika* 58:453–467
- 899 Gaillardet, J., Dupré, B., and Allègre, C.J., 1999. Geochemistry of large river suspended sediments:  
900 silicate weathering or recycling tracer? *Geochimica et Cosmochimica Acta* 63:4037–4051.
- 901 Garzanti, E., 2016. From static to dynamic provenance analysis—Sedimentary petrology upgraded.  
902 *Sedimentary Geology* 336:3-13.
- 903 Garzanti, E., 2017, The maturity myth in sedimentology and provenance analysis: *Journal of*  
904 *Sedimentary Research* 87:353-365.
- 905 Garzanti, E., 2019. Petrographic classification of sand and sandstone. *Earth-Science Reviews*  
906 192:545-563.
- 907 Garzanti, E., and Andò, S., 2007. Plate tectonics and heavy-mineral suites of modern sands. In:  
908 Mange, M.A., Wright, D.T. (eds.), *Heavy minerals in use*. Elsevier, Amsterdam, *Developments*  
909 *in Sedimentology* 58:741-763.
- 910 Garzanti, E., and Andò, S., 2019, Heavy Minerals for Junior Woodchucks: *Minerals* 9(3):148,

- 911 doi:10.3390/min9030148.
- 912 Garzanti, E., and Resentini, A., 2016. Provenance control on chemical indices of weathering (Taiwan  
913 river sands). *Sedimentary Geology* 336:81–95.
- 914 Garzanti, E., and Sternai, P., 2020. Against steady state: A quixotic plea for science. *Earth ArXiv*,  
915 <https://eartharxiv.org/p9xq7/>, doi:10.31223/osf.io/p9xq7
- 916 Garzanti, E., Vezzoli, G., Andò, S., and Castiglioni, G., 2001. Petrology of rifted-margin sand (Red  
917 Sea and Gulf of Aden, Yemen). *The Journal of Geology* 109:277–297.
- 918 Garzanti, E., Andò, S., and Vezzoli, G., 2006. The continental crust as a source of sand (Southern  
919 Alps cross-section, Northern Italy). *The Journal of Geology* 114:533–554.
- 920 Garzanti, E., Andò, S., and Vezzoli, G., 2009. Grain-size dependence of sediment composition and  
921 environmental bias in provenance studies. *Earth Planet. Sci. Lett.* 277:422–432.
- 922 Garzanti, E., Resentini, A., Vezzoli, G., Andò, S., Malusà, M.G., Padoan, M., and Paparella, P. 2010.  
923 Detrital fingerprints of fossil continental-subduction zones (axial belt provenance, European  
924 Alps). *The Journal of Geology* 118:341–362.
- 925 Garzanti, E., Resentini, A., Vezzoli, G., Andò, S., Malusà, M., and Padoan, M., 2012. Forward  
926 compositional modelling of Alpine orogenic sediments. *Sedimentary Geology* 280:149-164.
- 927 Garzanti, E., Vermeesch, P., Andò, S., Vezzoli, G., Valagussa, M., Allen, K., Khadi, K.A., and Al-  
928 Juboury, I.A., 2013a. Provenance and recycling of Arabian desert sand. *Earth Science Reviews*  
929 120:1–19.
- 930 Garzanti, E., Padoan, M., Andò, S., Resentini, A., Vezzoli, G., and Lustrino, M., 2013b. Weathering  
931 and relative durability of detrital minerals in equatorial climate: sand petrology and geochemistry  
932 in the East African Rift. *The Journal of Geology* 121:547–580.
- 933 Garzanti, E., Padoan, M., Setti, M., López-Galindo, A., and Villa, I.M., 2014a. Provenance versus  
934 weathering control on the composition of tropical river mud (southern Africa). *Chemical*  
935 *Geology* 366:61–74.
- 936 Garzanti, E., Vermeesch, P., Padoan, M., Resentini, A., Vezzoli, G., and Andò, S., 2014b. Provenance  
937 of passive-margin sand (southern Africa). *The Journal of Geology* 122:17-42.
- 938 Garzanti, E., Resentini, A., Andò, S., Vezzoli, G., and Vermeesch, P., 2015. Physical controls on sand  
939 composition and relative durability of detrital minerals during long-distance littoral and eolian  
940 transport (coastal Namibia). *Sedimentology* 62:971-996, doi:10.1111/sed.12169.



- 941 Garzanti, E., Dinis, P., Vermeesch, P., Andò, S., Hahn, A., Huvi, J., Limonta, M., Padoan, M.,  
942 Resentini, A., Rittner, M., and Vezzoli, G., 2018a, Dynamic uplift, recycling, and climate control  
943 on the petrology of passive-margin sand (Angola). *Sedimentary Geology* 375:86-104.
- 944 Garzanti, E., Andò, S., Limonta, M., Fielding, L., and Najman, Y., 2018b. Diagenetic control on  
945 mineralogical suites in sand, silt, and mud (Cenozoic Nile Delta): implications for provenance  
946 reconstructions. *Earth Sci. Rev.* 185:122–139.
- 947 Garzanti, E., Limonta, M., Vezzoli, G., An, W., Wang, J., and Hu, X., 2019a, Petrology and  
948 multiminerall fingerprinting of modern sand generated from a dissected magmatic arc (Lhasa  
949 River, Tibet), in Ingersoll, R.V., Lawton, T.F., and Graham, S.A., eds., *Tectonics, Sedimentary  
950 Basins, and Provenance: A Celebration of William R. Dickinson's Career*: Geological Society of  
951 America Special Paper 540:197-221, [https://doi.org/10.1130/2018.2540\(09\)](https://doi.org/10.1130/2018.2540(09)).
- 952 Garzanti, E., Andò, S., France-Lanord, C., Limonta, M., Borromeo, L., and Vezzoli, G., 2019b.  
953 Provenance of Bengal Shelf Sediments. 2. Petrology of sand. *Minerals* 9:642,  
954 doi:10.3390/min9100642.
- 955 Garzanti, E., Vermeesch, P., Andò, S., Botti, E., Limonta, M., Vezzoli, G., Dinis, P., Hahn, A.,  
956 Baudet, D., De Grave, J., and Kitambala Yaya, N., 2019c. Congo river sand and the equatorial  
957 quartz factory. *Earth-Science Reviews* 197:102918, [doi.org/10.1016/j.earscirev.2019.102918](https://doi.org/10.1016/j.earscirev.2019.102918)
- 958 Garzanti, E., He, J., Barbarano, M., Resentini, A., Li, C., Yang, L., Yang, S., and Wang, H., 2021a,  
959 Provenance versus weathering control on sediment composition in tropical monsoonal climate  
960 (South China) - 2. Sand petrology and heavy minerals. *Chemical Geology* 564, 119997  
961 doi.org/10.1016/j.chemgeo.2020.119997.
- 962 Garzanti, E., Dinis, P., Vezzoli, G., and Borromeo, L., 2021b. Sand and mud generation from Paraná-  
963 Etendeka continental flood basalts in contrasting climatic conditions (Uruguay vs. Namibia).  
964 *Sedimentology*, in press.
- 965 Garzanti, E., Bayon, G., Dennielou, B., Barbarano, M., Limonta, M., and Vezzoli, G., 2021c. The  
966 Congo deep-sea fan: Mineralogical, REE, and Nd-isotope variability in quartzose passive-margin  
967 sand. *Journal of Sedimentary Research* 91, doi:10.2110/jsr.2020.100
- 968 Garzanti, E., Bayon, G., Dinis, P., Vermeesch, P., Pastore, G., Resentini, A., Barbarano, M., Ncube,  
969 L., Van Niekerk, H.J., forthcoming .The segmented Zambezi sedimentary system from source to  
970 sink. 2. Geochemistry, clay minerals, and detrital zircon geochronology. *The Journal of Geology*.

- 971 Glynn, S.M., Master, S., Wiedenbeck, M., Davis, D.W., Kramers, J.D., Belyanin, G.A., Frei, D., and  
972 Oberthür, T., 2017. The Proterozoic Choma-Kalomo Block, SE Zambia: Exotic terrane or a  
973 reworked segment of the Zimbabwe Craton? *Precambrian Research* 298:421-438.
- 974 Goscombe, B., Foster, D.A., Gray, D., and Wade, B., 2020. Assembly of central Gondwana along the  
975 Zambezi Belt: Metamorphic response and basement reactivation during the Kuunga Orogeny.  
976 *Gondwana Research* 80:410-465.
- 977 Grantham, G.H., Marques, J., Wilson, M., Manhiça, V., and Hartzler, F., 2011. Explanation of the  
978 Geological Map of Mozambique, 1: 1 000 000. Direccção Nacional de Geologia, Maputo, 383 p.
- 979 Griffin, W.L., Powell, W.J., Pearson, N.J., and O'Reilly, S.Y., 2008. GLITTER: Data reduction  
980 software for laser ablation ICP-MS. In: Sylvester, P. (ed.), *Laser Ablation-ICP-MS in the Earth*  
981 *Sciences: Current Practices and Outstanding Issues*. Mineralogical Association of Canada, Short  
982 Course, Series 40:204–207.
- 983 Guillocheau, F., Chelalou, R., Linol, B., Dauteuil, O., Robin, C., Mvondo, F., Callec, Y., and Colin,  
984 J.P., 2015. Cenozoic landscape evolution in and around the Congo Basin: constraints from  
985 sediments and planation surfaces. In: de Wit, M.J., Guillocheau, F., de Wit, M.J.C. (Eds.),  
986 *Geology and Resource Potential of the Congo Basin, Regional Geology Reviews*. Springer-  
987 Verlag, Berlin Heidelberg, pp. 271–313.
- 988 Guillocheau, F., Simon, B., Baby, G., Bessin, P., Robin, C., and Dauteuil, O., 2018. Planation surfaces  
989 as a record of mantle dynamics: the case example of Africa. *Gondwana Research* 53:82–98.
- 990 Gumbrecht, T., McCarthy, T.S., and Merry, C.L., 2001. The topography of the Okavango Delta,  
991 Botswana, and its sedimentological and tectonic implications. *South African Journal of Geology*  
992 104:243–264.
- 993 Haddon, I.G., and McCarthy, T.S., 2005. The Mesozoic–Cenozoic interior sag basins of Central  
994 Africa: The Late-Cretaceous–Cenozoic Kalahari and Okavango basins. *J. Afr. Earth Sci.* 43:316-  
995 333.
- 996 Hanson, R.E. 2003. Proterozoic geochronology and tectonic evolution of southern Africa. In:  
997 Yoshida, M., Windley, B.F., Dasgupta, S. (eds.), *Proterozoic East Gondwana: supercontinent*  
998 *assembly and breakup*. Geol. Soc. London, Spec. Publ. 206:427-463.
- 999 Hanson, R.E., Harmer, R.E., Blenkinsop, T.G., Bullen, D.S., Dalziel, I.W.D., Gose, W.A., Hall, R.P.,  
1000 Kampunzu, A.B., Key, R.M., Mukwakwami, J., Munyanyiwa, H., Pancake, J.A., Seidel, E.K.,

- 1001 and Ward, S.E., 2006. Mesoproterozoic intraplate magmatism in the Kalahari Craton: a review.  
1002 *J. Afr. Earth Sci.* 46:141-167.
- 1003 Hargrove, U.S., Hanson, R.E., Martin, M.W., Blenkinsop, T.G., Bowring, S.A., Walker, N., and  
1004 Munyanyiwa, H., 2003. Tectonic evolution of the Zambezi orogenic belt: geochronological,  
1005 structural, and petrological constraints from northern Zimbabwe. *Precambrian Research* 123(2-  
1006 4):159-186.
- 1007 Hay, W.W., 1998. Detrital sediment fluxes from continents to oceans. *Chemical Geology* 145:287–  
1008 323.
- 1009 Hopper, E., Gaherty, J.B., Shillington, D.J., Accardo, N.J., Nyblade, A.A., Holtzman, B.K., Havlin,  
1010 C., Scholz, C.A., Chindandali, P.R., Ferdinand, R.W., and Mulibo, G.D., 2020. Preferential  
1011 localized thinning of lithospheric mantle in the melt-poor Malawi Rift. *Nature Geoscience* 13(8):  
1012 584-589.
- 1013 Hubert, J.F., 1962, A zircon–tourmaline–rutile maturity index and the interdependence of the  
1014 composition of heavy mineral assemblages with the gross composition and texture of sandstones:  
1015 *Journal of Sedimentary Petrology* 32:440–450.
- 1016 Ingersoll, R.V., Bullard, T.F., Ford, R.L., Grimm, J.P., Pickle, J.D., and Sares, S.W., 1984, The effect  
1017 of grain size on detrital modes: A test of the Gazzi-Dickinson point-counting method: *Journal of*  
1018 *Sedimentary Petrology* 54:103–116.
- 1019 Jacobs, J., Pisarevsky, S., Thomas, R.J., and Becker, T. 2008. The Kalahari Craton during the  
1020 assembly and dispersal of Rodinia. *Precambrian Res.* 160:142-158.
- 1021 Jelsma, H.A., and Dirks, P.H.G.M., 2002. Neoproterozoic tectonic evolution of the Zimbabwe Craton.  
1022 *In* Fowler, C.M.R.; Ebinger, C.J.; and Hawkesworth, C.J. (eds.), *The early Earth: physical,*  
1023 *chemical and biological development.* Geol. Soc. London, Spec. Publ. 199:183-211.
- 1024 John, T., Schenk, V., Haase, K., Scherer, E., and Tembo, F., 2003. Evidence for a Neoproterozoic  
1025 ocean in south-central Africa from mid-ocean-ridge-type geochemical signatures and pressure-  
1026 temperature estimates of Zambian eclogites. *Geology* 31:243-246.
- 1027 John, T., Schenk, V., Mezger, K., and Tembo, F., 2004. Timing and PT evolution of whiteschist  
1028 metamorphism in the Lufilian Arc–Zambezi Belt orogen (Zambia): Implications for the assembly  
1029 of Gondwana. *The Journal of Geology* 112(1):71-90.
- 1030 Johnson, M.R., Van Vuuren, C.J., Hegenberger, W.F., Key, R., and Show, U., 1996. Stratigraphy of  
1031 the Karoo Supergroup in southern Africa: an overview. *Journal of African Earth*

- 1032 Sciences 23(1):3-15.
- 1033 Jouet, G., and Deville, E., 2015 PAMELA-MOZ04 cruise, RV Pourquoi pas, [doi.org/10.17600/15000700](https://doi.org/10.17600/15000700).
- 1034 Jourdan, F., Féraud, G., Bertrand, H., Kampunzu, A.B., Tshoso, G., Watkeys, M.K., and Le Gall, B.,  
1035 2005. Karoo large igneous province: Brevity, origin, and relation to mass extinction questioned  
1036 by new  $^{40}\text{Ar}/^{39}\text{Ar}$  age data. *Geology* 33(9):745-748.
- 1037 Kampunzu, A.B., and Cailteux, J., 1999. Tectonic evolution of the Lufilian Arc (Central Africa  
1038 Copper Belt) during Neoproterozoic Pan African orogenesis. *Gondwana Research* 2(3):401-421.
- 1039 Kendall, J.M., and Lithgow-Bertelloni, C., 2016. Why is Africa rifting? In: Wright, T.J., Ayele, A.,  
1040 Ferguson, D.J., Kidane, T., Vye-Brown, C. (eds.), *Magmatic Rifting and Active Volcanism*.  
1041 Geological Society, London, Special Publications 420:11–30, [doi.org/10.1144/SP420.17](https://doi.org/10.1144/SP420.17).
- 1042 Key, R.M., Cotterill, F.P.D., and Moore, A.E., 2015. The Zambezi River: An archive of tectonic  
1043 events linked to the amalgamation and disruption of Gondwana and subsequent evolution of the  
1044 African Plate. *South African Journal of Geology* 118(4):425-438.
- 1045 Kinabo, B.D., Atakwana, E.A., Hogan, J.P., Modisi, M.P., Wheaton, D.D., and Kampunzu, A.B.,  
1046 2007. Early structural development of the Okavango rift zone, NW Botswana. *Journal of African*  
1047 *Earth Sciences* 48:125–136.
- 1048 Klimke, J., Franke, D., Gaedicke, C., Schreckenberger, B., Schnabel, M., Stollhofen, H., Rose, J., and  
1049 Chaheire, M., 2016. How to identify oceanic crust—Evidence for a complex break-up in the  
1050 Mozambique Channel, off East Africa *Tectonophysics* 693:436–452.
- 1051 Knight, J., and Grab, S.W., 2018. The geomorphic evolution of southern Africa during the Cenozoic.  
1052 In: Holmes, P.J., Boardman, J. (eds.), *Southern African Landscapes and Environmental Change*.  
1053 Routledge, ch.2, pp. 6-28.
- 1054 Kokonyangi, J.W., Kampunzu, A.B., Armstrong, R., Yoshida, M., Okudaira, T., Arima, M., and  
1055 Ngulube, D.A., 2006. The Mesoproterozoic Kibaride belt (Katanga, SE DR Congo). *Journal of*  
1056 *African Earth Sciences* 46(1-2):1-35.
- 1057 Kolla, V., Kostecky, J.A., Henderson, L., and Hess, L., 1980. Morphology and Quaternary  
1058 sedimentation of the Mozambique Fan and environs, southwestern Indian Oceans.  
1059 *Sedimentology* 27:357-378.
- 1060 König, M., and Jokat, W., 2010. Advanced insights into magmatism and volcanism of the  
1061 Mozambique Ridge and Mozambique Basin in the view of new potential field data. *Geophysical*

- 1062 Journal International 180(1):158-180.
- 1063 Kottek, M., Grieser, J., Beck, C., Rudolf, B., and Rubel, F., 2006. World map of the Köppen–Geiger  
1064 climate classification updated. *Meteorologische Zeitschrift* 15:259–263.
- 1065 Krynine, P.D., 1948. The megascopic study and field classification of sedimentary rocks. *The Journal*  
1066 *of Geology* 56:130-165.
- 1067 Leopold, L.B., Wolman, M.G., and Miller, J.P., 1995. *Fluvial Processes in Sedimentology*. Dover  
1068 Publications, New York, 522 p.
- 1069 Le Pera, E., and Morrone, C., 2020. The use of mineral interfaces in sand-sized volcanic rock  
1070 fragments to infer mechanical durability. *Journal of Palaeogeography* 9(1): 1-26.
- 1071 Lithgow-Bertelloni, C., and Silver, P.G., 1998. Dynamic topography, plate driving forces and the  
1072 African superswell. *Nature* 395(6699):269-272.
- 1073 Macgregor, D., 2018. History of the development of Permian–Cretaceous rifts in East Africa: a series  
1074 of interpreted maps through time. Thematic set: Tectonics and petroleum systems of East Africa.  
1075 Geological Society London, *Petroleum Geoscience* 24:8-20, doi/10.1144/petgeo2016-155.
- 1076 Main, M., 1990. *Zambezi. Journey of a river*. Southern Book Publishers, Halfway Housem, South  
1077 Africa, 313 p.
- 1078 Majaule, T., Hanson, R.E., Key, R.M., Singletary, S.J., Martin, M.W., and Bowring, S.A., 2001. The  
1079 Magondi Belt in northeast Botswana: regional relations and new geochronological data from the  
1080 Sua Pan area. *Journal of African Earth Sciences* 32:257-267.
- 1081 Malusà, M.G., Resentini, A., and Garzanti, E., 2016. Hydraulic sorting and mineral fertility bias in  
1082 detrital geochronology. *Gondwana Research* 31:1-19.
- 1083 Manninen, T., Eerola, T., Makitie, H., Vuori, S., Luttinen, A., Sérvano, A., and Manhiça, V., 2008.  
1084 The Karoo volcanic rocks and related intrusions in southern and central Mozambique. *Geol.*  
1085 *Surv. Finland, Special Paper* 48:211-250.
- 1086 Maselli, V., Kroon, D., Iacopini, D., Wade, B.S., Pearson, P.N., and de Haas, H., 2019. Impact of the  
1087 East African Rift System on the routing of the deep- water drainage network offshore Tanzania,  
1088 western Indian Ocean. *Basin Research*, doi: 10.1111/bre.12398.
- 1089 Master, S., Bekker, A., and Hofmann, A., 2010. A review of the stratigraphy and geological setting  
1090 of the Palaeoproterozoic Magondi Supergroup, Zimbabwe–Type locality for the Lomagundi  
1091 carbon isotope excursion. *Precambrian Research* 182(4):254-273.

- 1092 Milliken, K.L., 2007. Provenance and diagenesis of heavy minerals, Cenozoic units of the  
1093 northwestern Gulf of Mexico sedimentary basin In: Mange, M.A., Wright, D.T. (eds.), Heavy  
1094 minerals in use. Elsevier, Amsterdam, *Developments in Sedimentology* 58: 247-261.
- 1095 Miramontes, E., Jouet, G., Thereau, E., Bruno, M., Penven, P., Guerin, C., Le Roy, P., Droz, L., Jorry,  
1096 S.J., Hernández-Molina, F.J., Thiéblemont, A., Silva Jacinto, R., Cattaneo, A., 2020. The impact  
1097 of internal waves on upper continental slopes: Insights from the Mozambican margin (southwest  
1098 Indian Ocean). *Earth Surface Processes and Landforms* 45(6), 1469-1482.
- 1099 Modisi, M.P., Atekwana, E.A., Kampunzu, A.B., and Ngwisanyi, T.H., 2000. Rift kinematics during  
1100 the incipient stages of continental extension: Evidence from the nascent Okavango rift basin,  
1101 northwest Botswana. *Geology* 28:939–942.
- 1102 Moore, A.E., and Blenkinsop, T. 2002. The role of mantle plumes in the development of continental-  
1103 scale drainage patterns: The southern African example revisited. *South African Journal of*  
1104 *Geology* 105:353–360.
- 1105 Moore, A.E., and Dingle, R.V., 1998. Evidence for fluvial sediment transport of Kalahari sands in  
1106 central Botswana. *S. Afr. J. Geol.* 101:143–153.
- 1107 Moore, A.E., and Larkin, P.A., 2001. Drainage evolution in south-central Africa since the breakup of  
1108 Gondwana. *South African Journal of Geology* 104:47–68.
- 1109 Moore, A.E., Cotterill, F.P.D., Main, M.P.L., and Williams, H.B., 2007. The Zambezi River. In:  
1110 Gupta, A. (ed.), *Large Rivers: Geomorphology and Management*. Wiley, Chichester, pp. 311–  
1111 332.
- 1112 Moore, A.E., Cotterill, F.P.D., Broderick, T.G., and Plowes, D., 2009a. Landscape evolution in  
1113 Zimbabwe from the Permian to present, with implications for kimberlite prospecting. *South*  
1114 *African Journal of Geology* 112:65–86.
- 1115 Moore, A., Blenkinsop, T., and Cotterill, F.P.D., 2009b. Southern African topography and erosion  
1116 history: plumes or plate tectonics? *Terra Nova* 21:310–315.
- 1117 Morrone, C., Le Pera, E., Marsaglia, K.M., and De Rosa, R., 2020. Compositional and textural study  
1118 of modern beach sands in the active volcanic area of the Campania region (southern Italy).  
1119 *Sedimentary Geology* 396:105567.
- 1120 Morton, A.C., and Hallsworth, C., 2007. Stability of detrital heavy minerals during burial diagenesis.  
1121 In: Mange, M.A., Wright, D.T. (eds.), *Heavy Minerals in Use*. Elsevier, Amsterdam,  
1122 *Developments in Sedimentology* 58: 215-245.

- 1123 Nechaev, V.P., and Isphording, W.C., 1993. Heavy mineral assemblages of continental margins as  
1124 indicators of plate-tectonic environments. *Journal of Sedimentary Petrology* 63:1110–1117.
- 1125 Nesbitt, H.W., and Young, G.M., 1982. Early Proterozoic climates and plate motions inferred from  
1126 major element chemistry of lutites. *Nature* 299:715–717.
- 1127 Nyambe, I.A., and Utting, J., 1997. Stratigraphy and palynostratigraphy, Karoo Supergroup (Permian  
1128 and Triassic), mid-Zambezi Valley, southern Zambia. *South African Journal of Geology* 24:563–  
1129 583.
- 1130 O'Connor, P.W., and Thomas, D.S.G., 1999. The timing and environmental significance of Late  
1131 Quaternary linear dune development in western Zambia. *Quaternary Research* 52:44–55.
- 1132 Partridge, T.C., and Maud, R.R., 1987. Geomorphic evolution of southern Africa since the Mesozoic.  
1133 *South African Journal of Geology* 90(2):179-208.
- 1134 Pastore, G., Baird, T., Vermeesch, P., Resentini, A., and Garzanti, E., 2021. Provenance and recycling  
1135 of Sahara desert sand. *Earth-Science Reviews* 216:103606,  
1136 doi.org/10.1016/j.earscirev.2021.103606
- 1137 Phethean, J.J.J., Kalnins, L.M., van Hunen, J., Biffi, P.G., Davies, R.J., and McCaffrey, K.J.W., 2016.  
1138 Madagascar's escape from Africa: A high-resolution plate reconstruction for the Western Somali  
1139 Basin and implications for supercontinent dispersal, *Geochemistry Geophysics Geosystems* 17:  
1140 5036–5055.
- 1141 Potter, P.E., 1978. Petrology and chemistry of modern big river sands. *The Journal of Geology* 86:  
1142 423–449.
- 1143 Resentini, A., Goren, L., Castelltort, S., and Garzanti, E., 2017. Partitioning the sediment flux by  
1144 provenance and tracing erosion patterns in Taiwan. *Journal Geophysical Research - Earth Surface*  
1145 122(7):1430-1454, doi:10.1002/2016JF004026.
- 1146 Rieu, R., Allen, P.A., Plötze, M., and Pettke, T., 2007. Compositional and mineralogical variations  
1147 in a Neoproterozoic glacially influenced succession, Mirbat area, South Oman: Implications for  
1148 paleoweathering conditions. *Precambrian Research* 154:248–265.
- 1149 Roberts, E.M., Stevens, N.J., O'Connor, P.M., Dirks, P.H.G.M., Gottfried, M.D., Clyde, W.C.,  
1150 Armstrong, R.A., Kemp, A.I.S., and Hemming, S., 2012. Initiation of the western branch of the  
1151 East African Rift coeval with the eastern branch. *Nature Geoscience* 5(4):289-294.
- 1152 Russell, R.D., 1937, Mineral composition of Mississippi River sands. Geological Society of America,

- 1153 Bulletin 48:1307–1348.
- 1154 Salman, G., and Abdula, I., 1995. Development of the Mozambique and Ruvuma sedimentary basins,  
1155 offshore Mozambique. *Sedimentary Geology* 96:7-41.
- 1156 Schulz, H., Lückge, A., Emeis, K.C., and Mackensen, A., 2011. Variability of Holocene to Late  
1157 Pleistocene Zambezi riverine sedimentation at the upper continental slope off Mozambique, 15°-  
1158 21°S. *Marine Geology* 286:21–34.
- 1159 Schwanghart, W., and Scherler, D., 2014. TopoToolbox 2 – MATLAB-based software for  
1160 topographic analysis and modeling in Earth surface sciences. *Earth Surface Dynamics* 2:1-7,  
1161 doi:10.5194/esurf-2-1-2014.
- 1162 Shaw, A., and Goudie, A.S., 2002. Geomorphological evidence for the extension of the Mega-  
1163 Kalahari into south-central Angola. *S. Afr. Geogr. J.* 84:182–194.
- 1164 Shaw, P., and Thomas, D.S.G., 1988. Lake Caprivi: a late Quaternary link between the Zambezi and  
1165 middle Kalahari drainage. *Z. Geomorphol.* 32:329–337.
- 1166 Shukri, N.M., 1950. The mineralogy of some Nile sediments. *Quarterly Journal of the Geological*  
1167 *Society London* 105:511–534.
- 1168 Shvetsov, M.S., 1934. Petrografiya osadochnykh porod (Petrography of Sedimentary Rocks).  
1169 Moscow-Leningrad: Gostoptekhizdat (1948), 387 p. (in Russian)
- 1170 Söderlund, U., Hofmann, A., Klausen, M.B., Olsson, J.R., Ernst, R.E., and Persson, P.O., 2010.  
1171 Towards a complete magmatic barcode for the Zimbabwe craton: Baddeleyite U–Pb dating of  
1172 regional dolerite dyke swarms and sill complexes. *Precambrian Research* 183(3):388-398.
- 1173 Stokes, S., Haynes, G., Thomas, D.S.G., Horrocks, J.L., Higginson, M., and Malifa, M., 1998.  
1174 Punctuated aridity in southern Africa during the last glacial cycle: The chronology of linear dune  
1175 construction in the northeastern Kalahari. *Palaeogeography Palaeoclimatology Palaeoecology*  
1176 137:305–322.
- 1177 Svensen, H., Corfu, F., Polteau, S., Hammer, Ø., and Planke, S. 2012. Rapid magma emplacement in  
1178 the Karoo Large Igneous Province. *Earth Planet. Sci. Lett.* 325/326:1-9.
- 1179 Taylor, S.R., and McLennan, S.M., 1995. The geochemical evolution of the continental crust.  
1180 *Reviews of Geophysics* 33:241–265.
- 1181 Thomas, D.S.G., and Shaw, P.A., 1988. Late Cainozoic drainage evolution in the Zambezi basin:  
1182 evidence from the Kalahari rim. *Journal of African Earth Sciences* 7:611–618.



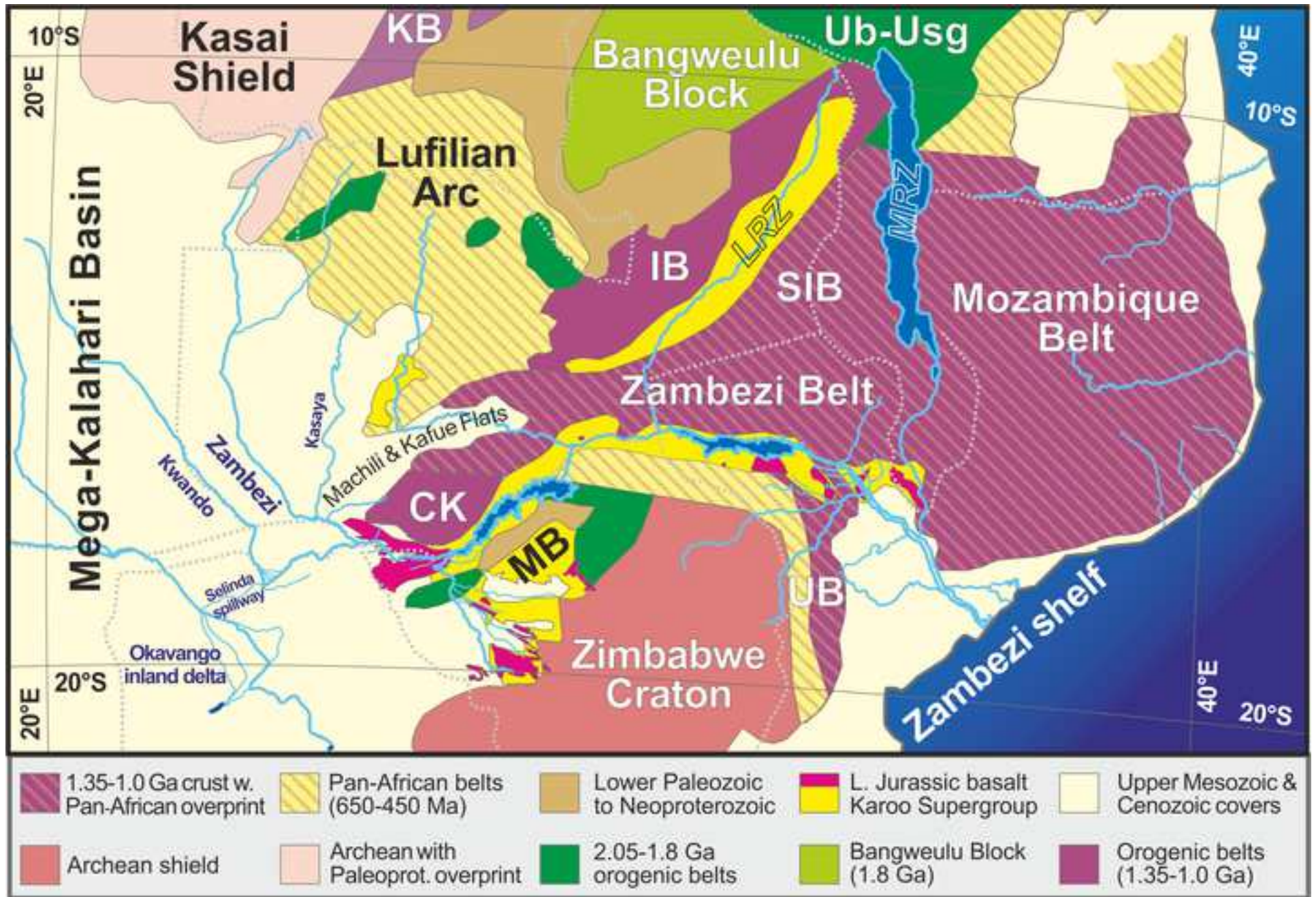
- 1183 Thomas, D.S.G., and Shaw, P.A., 1991. *The Kalahari Environment*. Cambridge University Press,  
1184 Cambridge, UK, 284 p.
- 1185 Thomas, D.S.G., and Shaw, P.A., 2002. Late Quaternary environmental change in central southern  
1186 Africa: new data, synthesis, issues and prospects. *Quaternary Sci. Rev.* 21:783-797.
- 1187 Thomas, D.S.G.; O'Connor, P.W.; Bateman, M.D.; Shaw, P.A.; Stokes, S.; and Nash, D.J., 2000.  
1188 Dune activity as a record of late Quaternary aridity in the northern Kalahari: new evidence from  
1189 northern Namibia interpreted in the context of regional arid and humid chronologies.  
1190 *Palaeogeogr. Palaeoclimatol. Palaeoecol.* 156:243–259.
- 1191 Vallier, T.L., 1974. Volcanogenic sediments and their relation to landmass volcanism and sea floor-  
1192 continent movements, western Indian Ocean. *Leg 25, Init. Rep. D.S.D.P.* 25:515–542.
- 1193 van der Lubbe, J.J.L., Tjallingii, R., Prins, M.A., Brummer, G.J.A., Jung, S.J.A., Kroon, D., and  
1194 Schneider, R.R., 2014. Sedimentation patterns off the Zambezi River over the last 20,000 years.  
1195 *Marine Geology* 355:189–201.
- 1196 von Eynatten, H., Pawlowsky-Glahn, V., and Egozcue, J.J., 2002. Understanding perturbation on the  
1197 simplex: a simple method to better visualise and interpret compositional data in ternary diagrams.  
1198 *Mathematical Geology* 34:249–257.
- 1199 Vormann, M., Franke, D., and Jokat, W., 2020. The crustal structure of the southern Davie Ridge  
1200 offshore northern Mozambique – A wide-angle seismic and potential field study. *Tectonophysics*  
1201 778:228370.
- 1202 Walford, H.L., White, N.J., and Sydow, J.C., 2005. Solid sediment load history of the Zambezi Delta.  
1203 *Earth and Planetary Science Letters* 238:49–63.
- 1204 Wellington, J. 1955. *Southern Africa: A geographical study. Physical geography, climate, vegetation*  
1205 *and soils: hydrography, V.1*. Cambridge, UK, Cambridge University Press, 528 p.
- 1206 Whipple, K.X., 2004. Bedrock rivers and the geomorphology of active orogens. *Annual Reviews*  
1207 *Earth Planetary Sciences* 32:151–185.
- 1208 Zindorf, M., Rooze, J., Meille, C., März, C., Jouet, G., Newton, R., Brandily, C., and Pastor, L., 2021.  
1209 The evolution of early diagenetic processes at the Mozambique margin during the last glacial-  
1210 interglacial transition. *Geochimica et Cosmochimica Acta* 300:9-94.

Figure 1

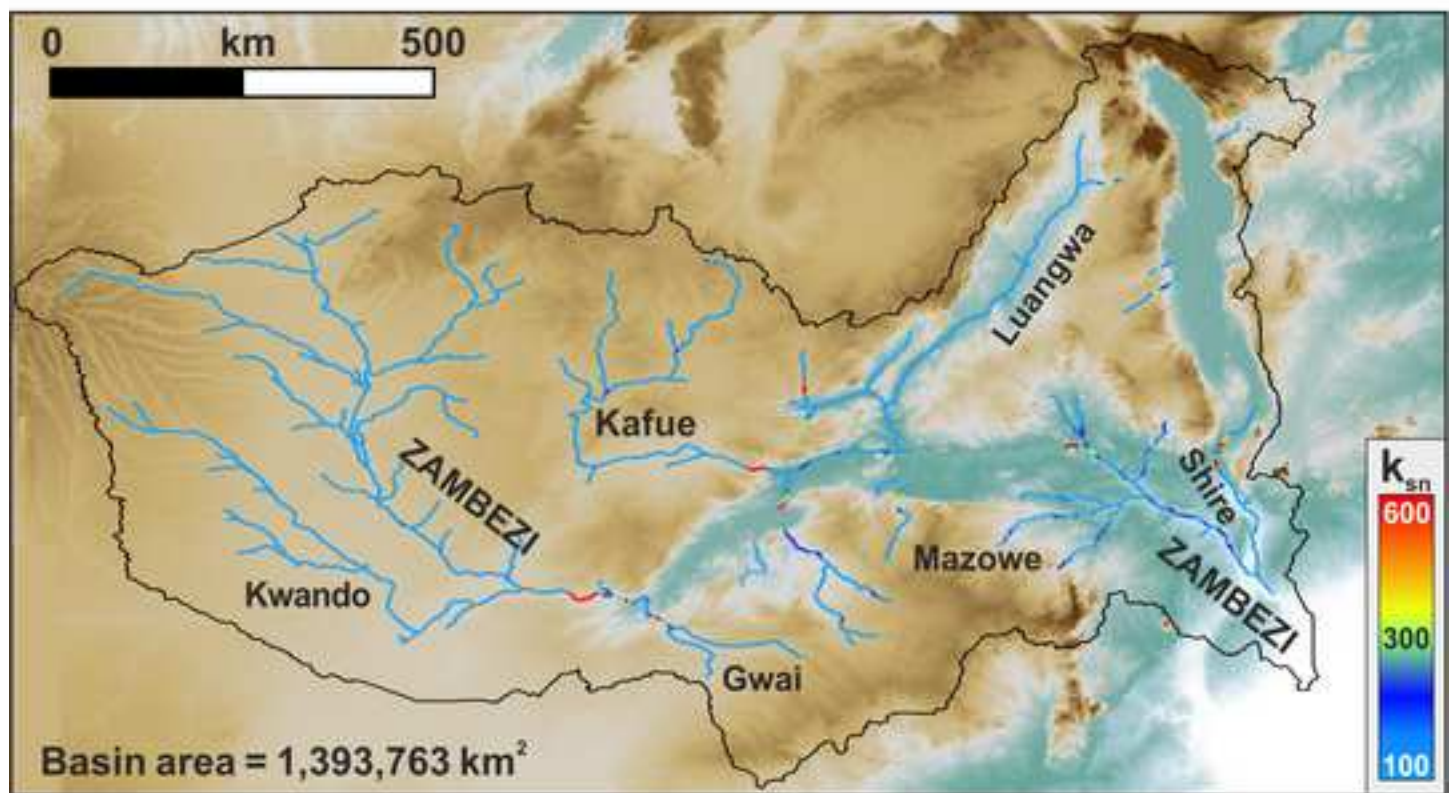
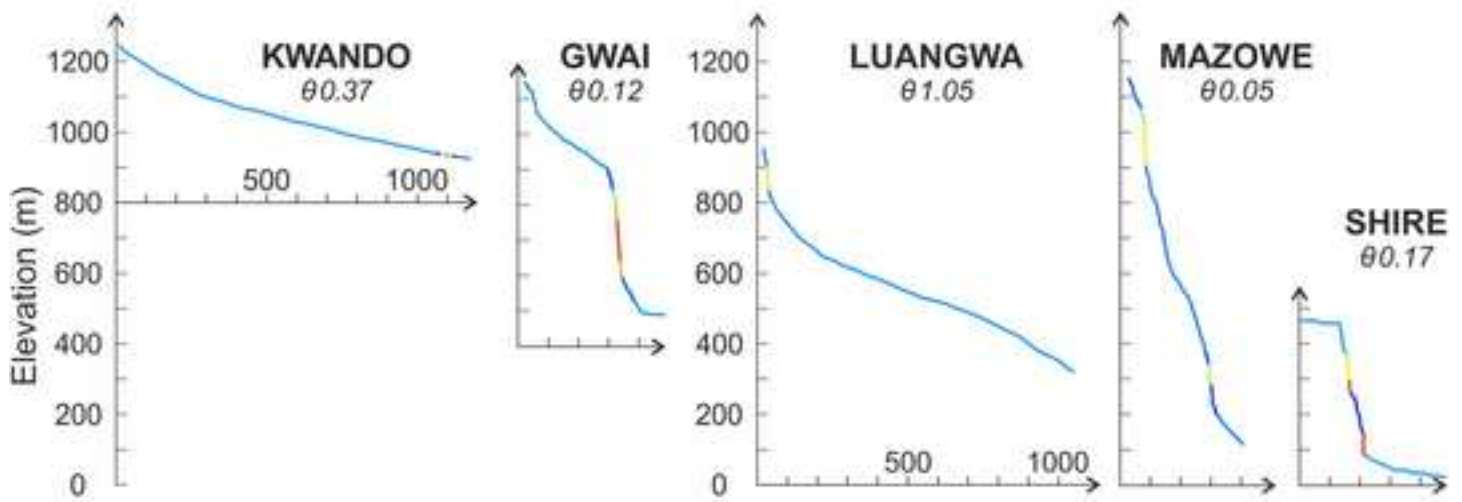
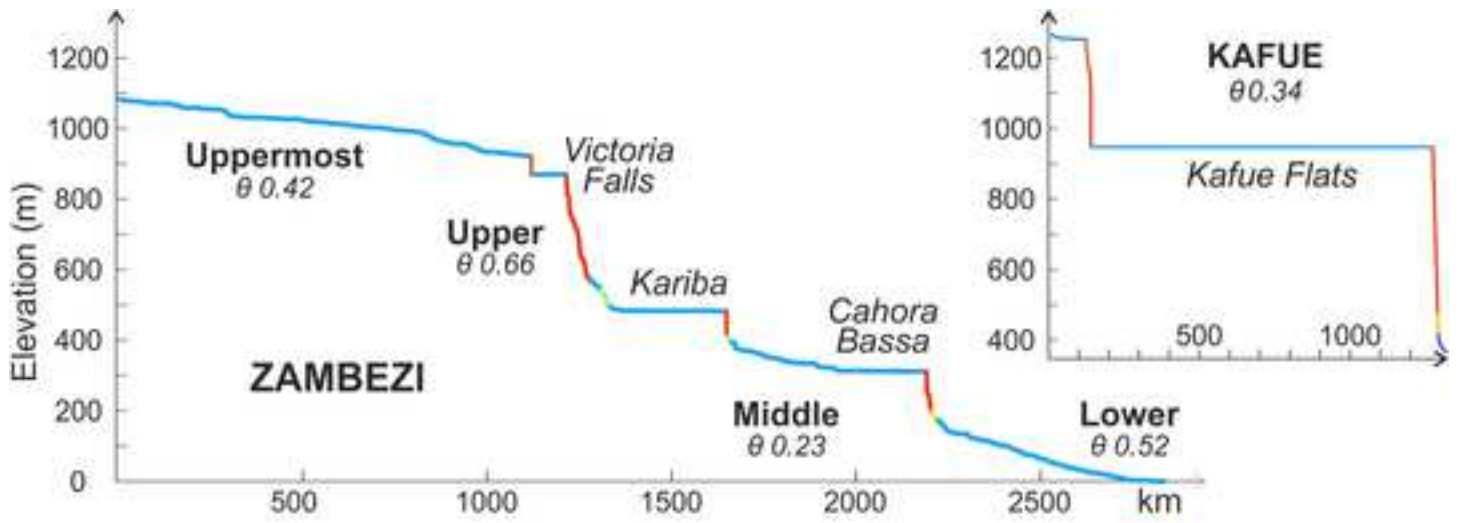




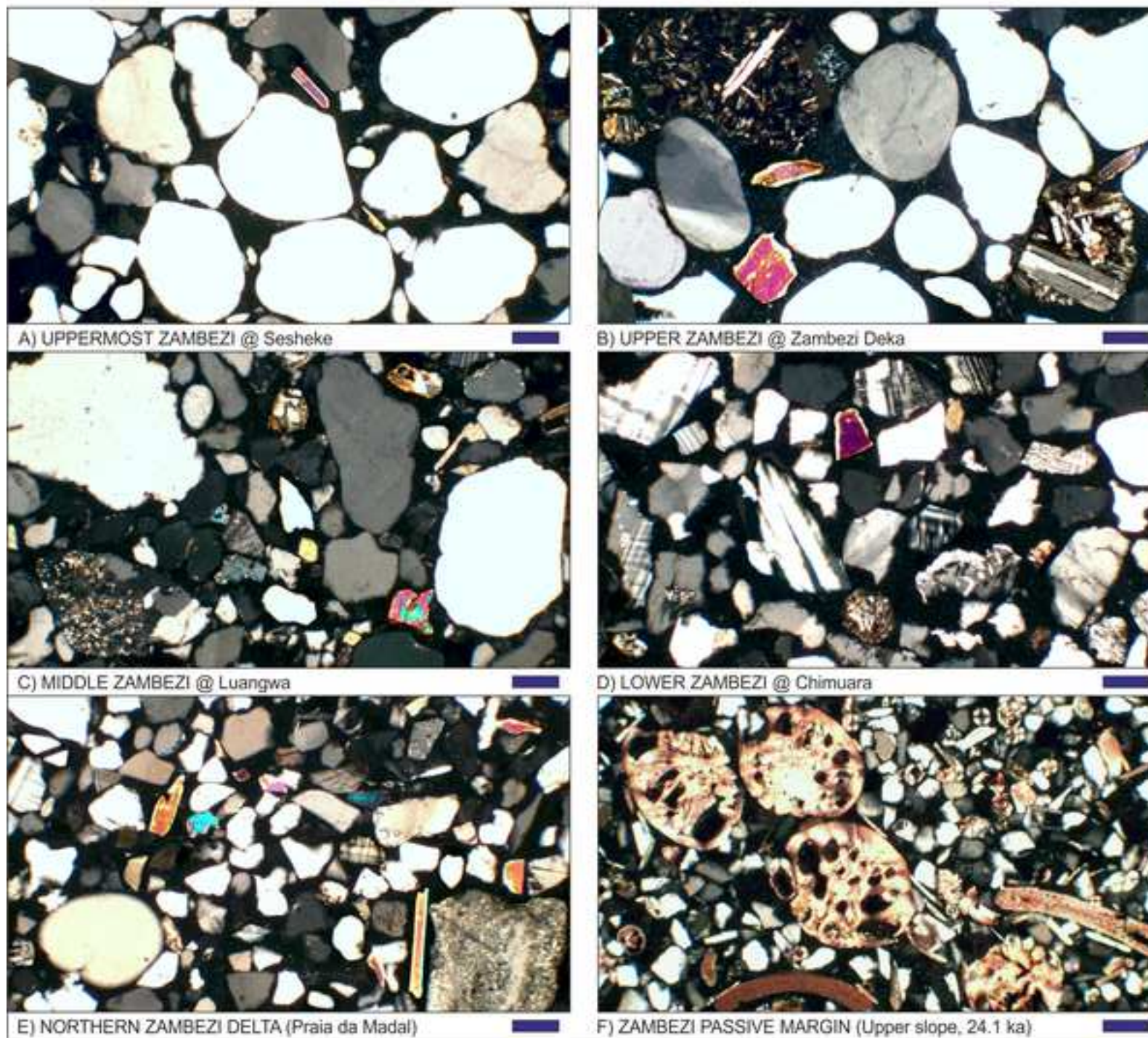
Figure 2



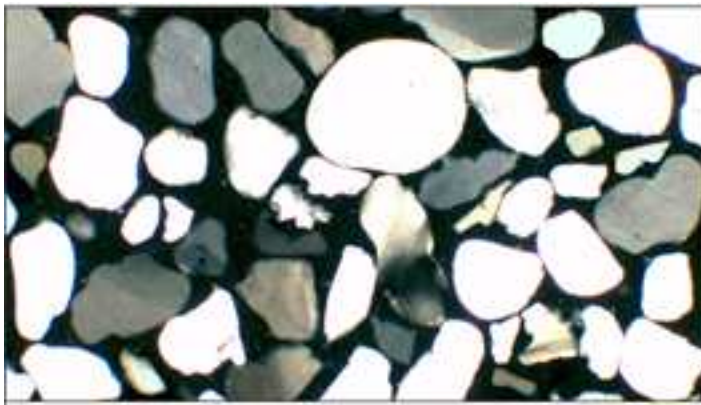




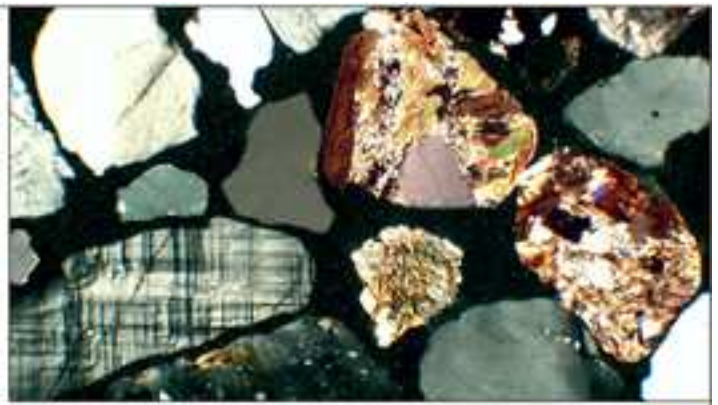




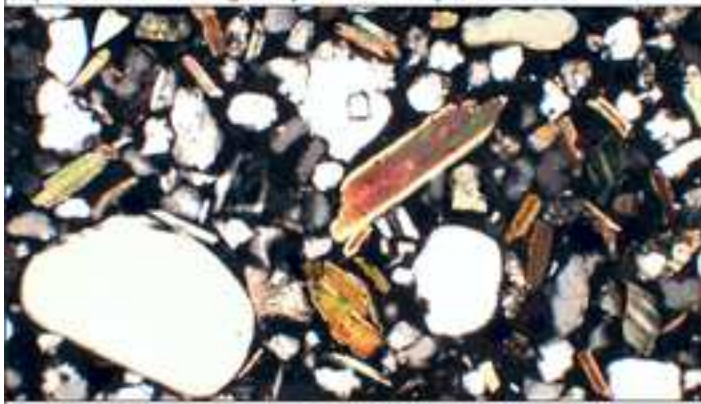




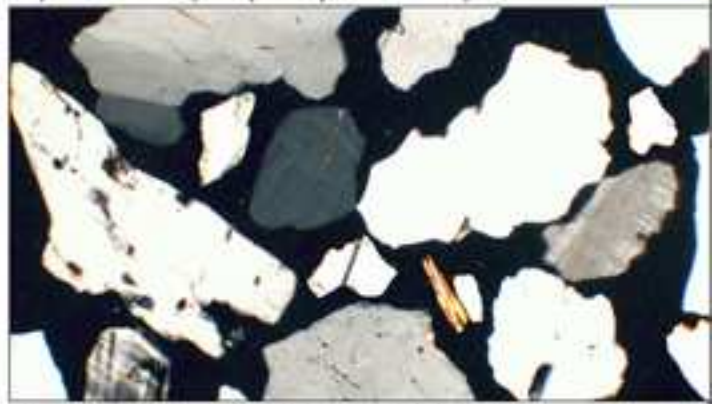
A) KWANDO RIVER (pure quartzose sand)



B) GWAI RIVER (feldspatho-quartzose sand)



C) KAFUE RIVER (feldspatho-quartzose micaceous sand)



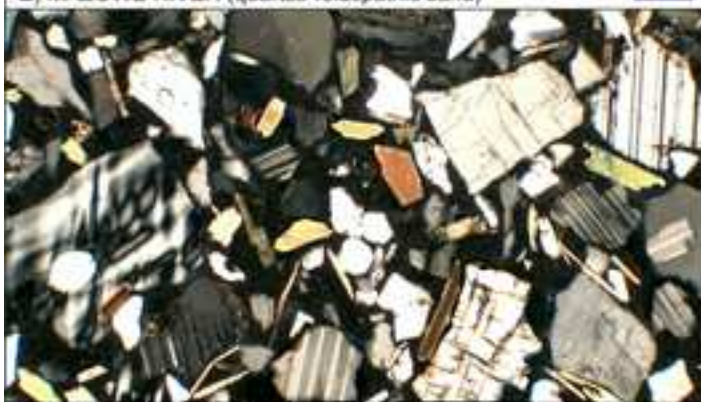
D) LUANGWA RIVER (feldspatho-quartzose sand)



E) MAZOWE RIVER (quartzo-feldspathic sand)



F) MORRUNGUZE RIVER (quartzo-feldspathic sand)

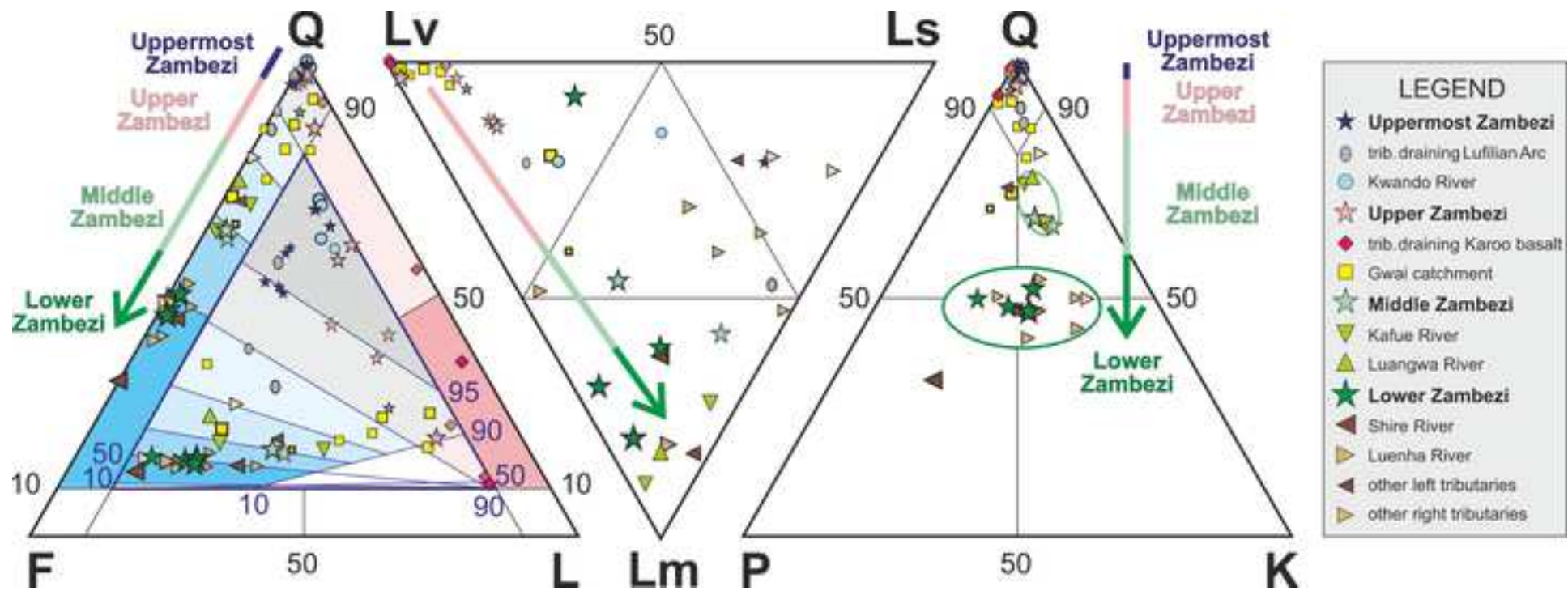


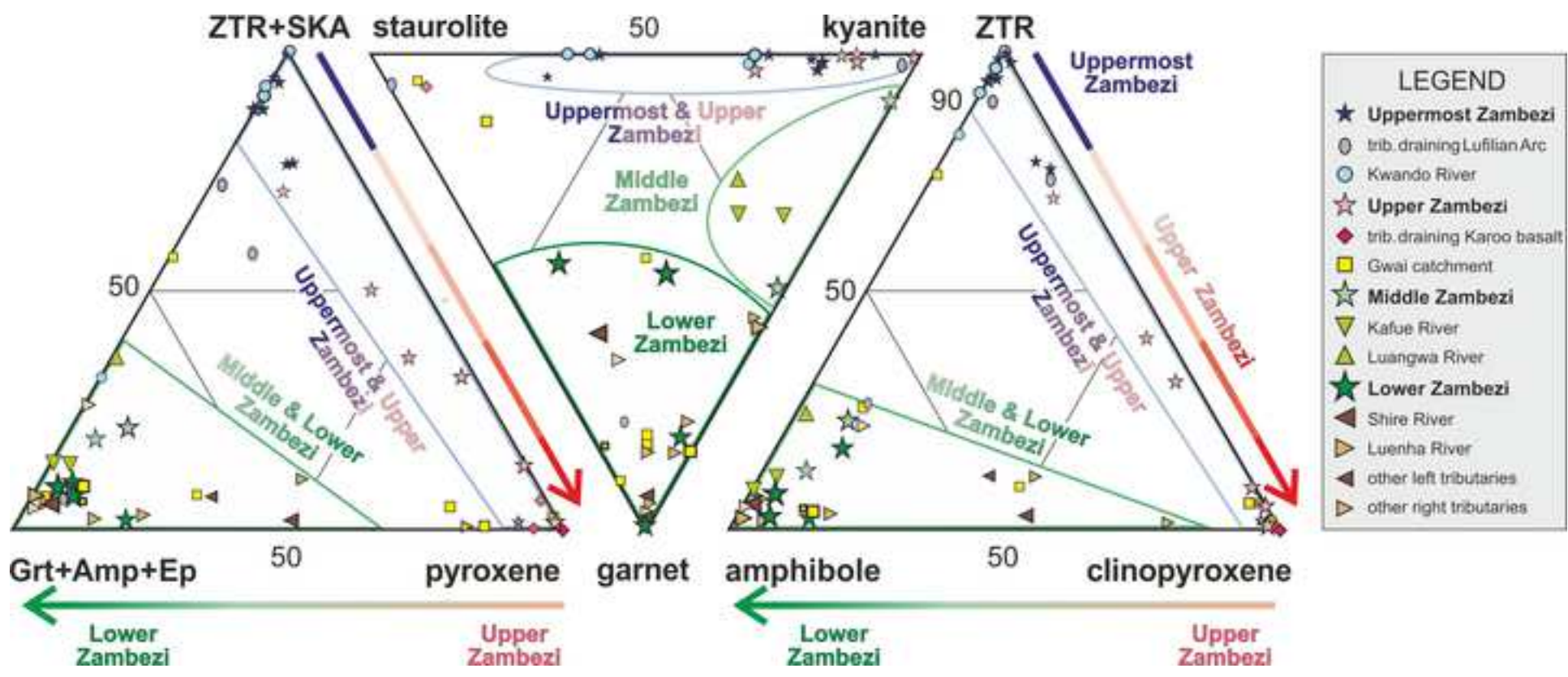
G) SHIRE RIVER (quartzo-feldspathic sand)



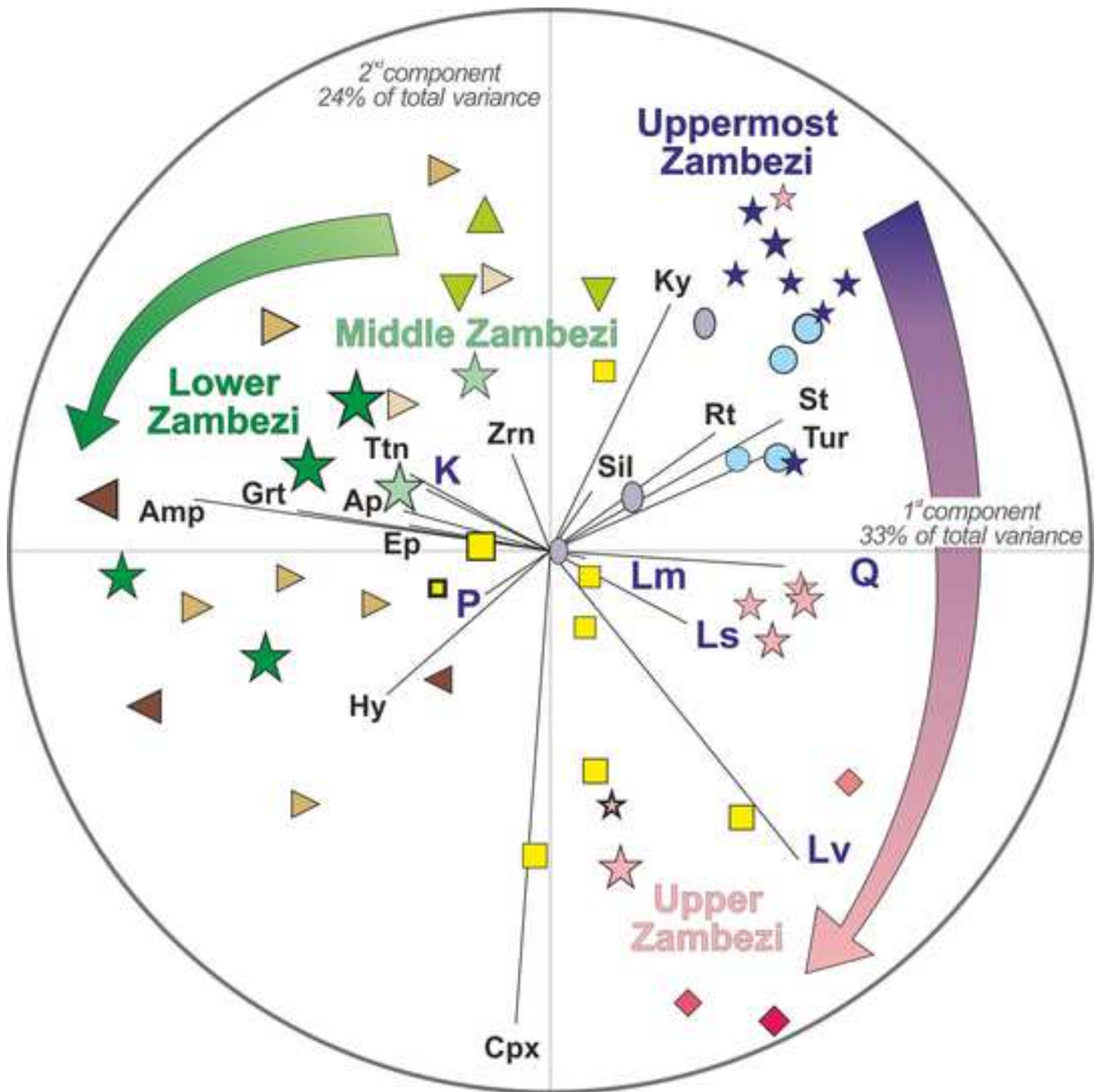
H) ZANGUE RIVER (quartz-rich feldspatho-quartzose sand)











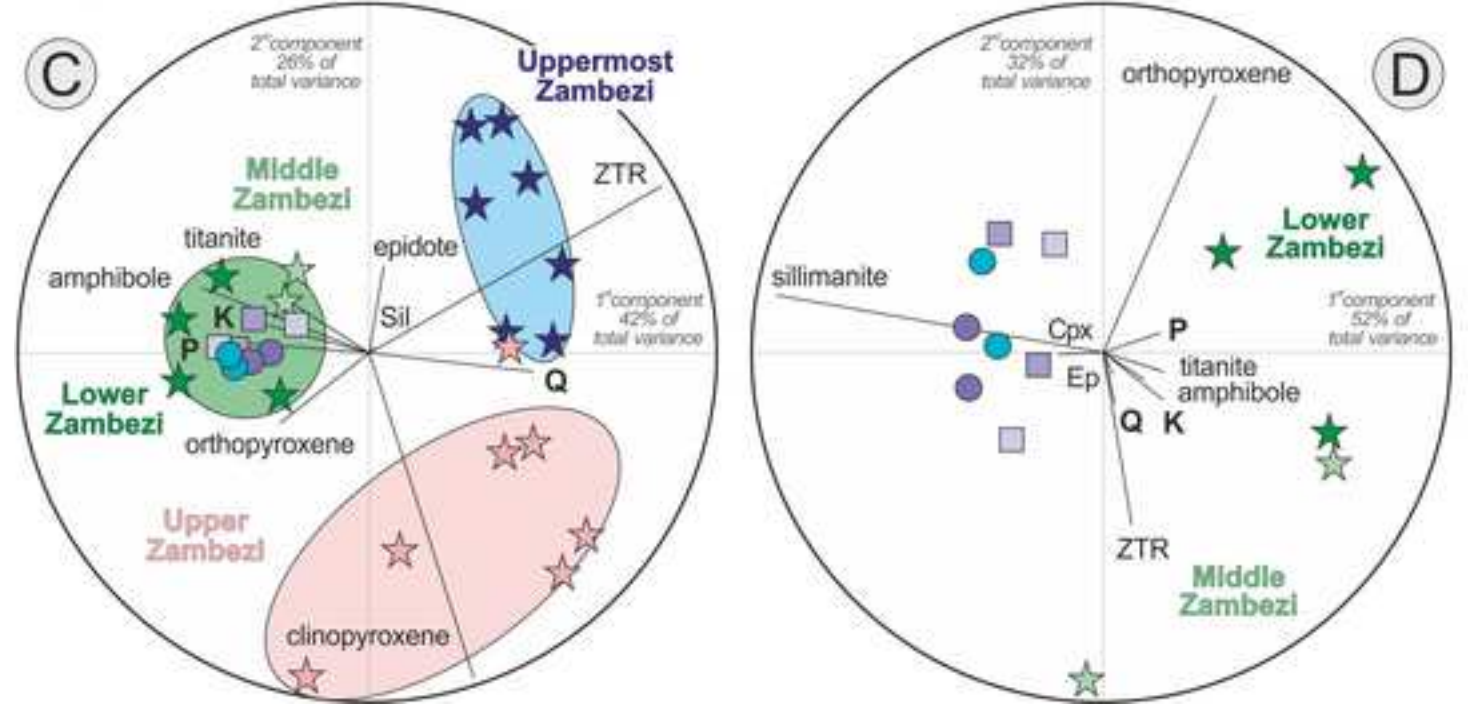
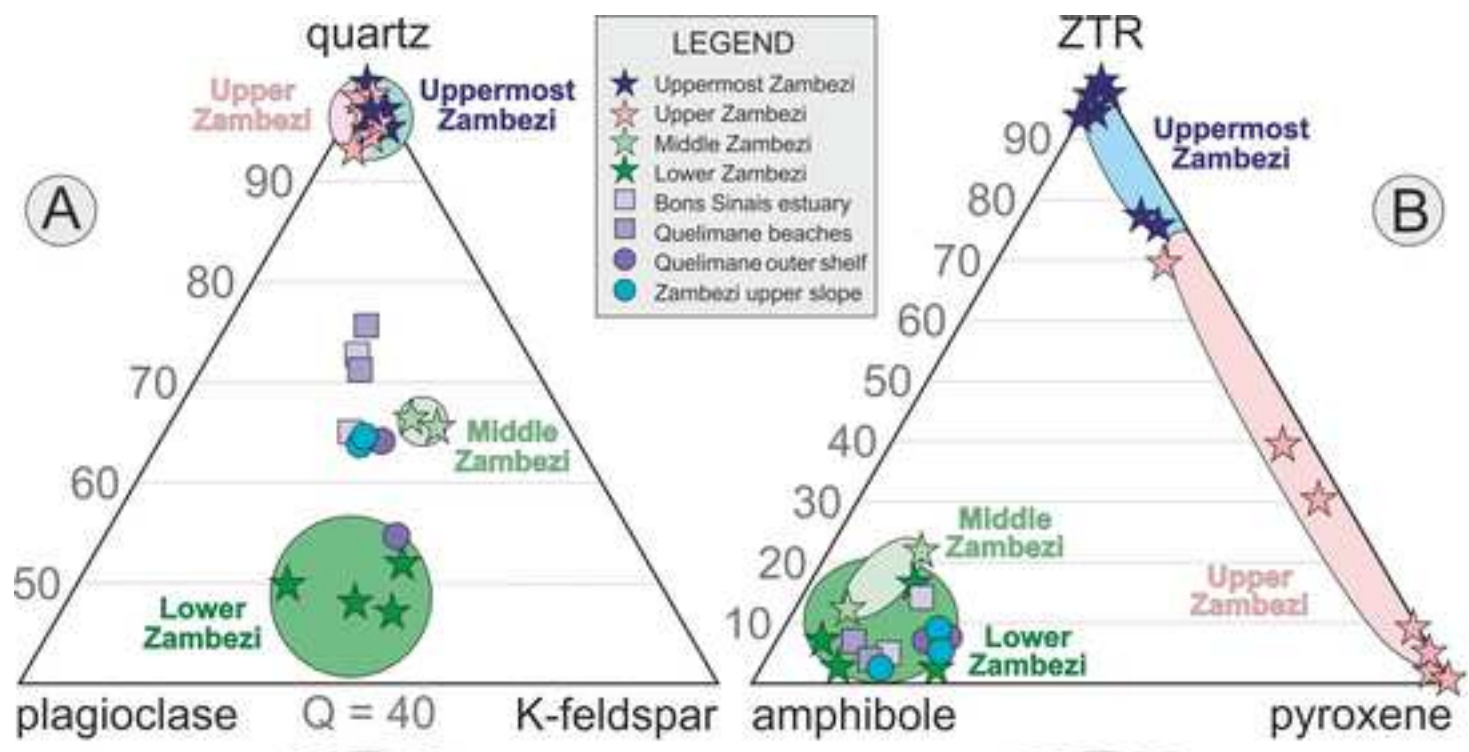


Table 1

RIVER	n°	Q	F	Lvm	Lsm	Lmfb	P/F	mica	tHMC	ZTR	Ap	Ttn	Ep	Grt	St	Ky	Sil	Amp	Cpx	Hy	&tHM	ACI		
Kwando River	3	99	1	0	0	0	100.0	n.d.	0%	0.1	61	0.3	0.3	3	0	16	16	0	2	0	0	1	100.0	39
& U <sup>st</sup> Z. tributaries	3	90	9	0.2	0.5	0	100.0	36%	2%	0.4	31	1	1	38	2	5	6	1	7	5	2	2	100.0	0-5
<b>Uppermost Zambezi</b>	<b>6</b>	<b>96</b>	<b>3</b>	<b>0</b>	<b>0</b>	<b>0</b>	100.0	<b>32%</b>	<b>0.1%</b>	<b>0.4</b>	<b>60</b>	<b>0</b>	<b>0.4</b>	<b>5</b>	<b>0.3</b>	<b>7</b>	<b>18</b>	<b>0</b>	<b>2</b>	<b>4</b>	<b>0</b>	<b>2</b>	100.0	<b>0</b>
U.Z. tributaries pre-VF	1	91	1	7	1	0	100.0	n.d.	0%	0.3	5	0.4	0	0.4	0	1	0	0	0.4	92	0	0	100.0	n.d.
<b>Upper Zambezi pre-VF</b>	<b>4</b>	<b>96</b>	<b>2</b>	<b>1</b>	<b>0</b>	<b>0.2</b>	100.0	<b>47%</b>	<b>0%</b>	<b>0.4</b>	<b>34</b>	<b>0</b>	<b>0</b>	<b>8</b>	<b>0.2</b>	<b>3</b>	<b>23</b>	<b>0.5</b>	<b>3</b>	<b>27</b>	<b>0</b>	<b>1</b>	100.0	<b>0-39</b>
U.Z. tributaries pre-Kariba	2	46	2	52	0	0	100.0	n.d.	0%	10.5	0	0	0	3	0	0	0	0	0	97	0	0	100.0	n.d.
<b>Upper Zambezi pre-Kariba</b>	<b>4</b>	<b>93</b>	<b>3</b>	<b>4</b>	<b>0</b>	<b>0</b>	100.0	<b>60%</b>	<b>0%</b>	<b>1.3</b>	<b>3</b>	<b>0.3</b>	<b>0</b>	<b>2</b>	<b>0.2</b>	<b>2</b>	<b>6</b>	<b>0</b>	<b>1</b>	<b>84</b>	<b>0</b>	<b>1</b>	100.0	n.d.
Gwai River	3	74	22	3	1	1	100.0	61%	4%	1.6	3	1	0	18	7	0.3	1	1	35	30	0.2	1	100.0	11-37
Gwai tributaries	5	83	11	5	0.5	0	100.0	60%	0%	3.5	12	1	2	27	2	1	0.2	0	12	43	0	0.4	100.0	8-34
Kafue	2	67	29	0.4	0.5	3	100.0	41%	6%	6.7	8	2	3	10	2	1	4	1	67	1	0	1	100.0	9-16
<b>Middle Zambezi</b>	<b>2</b>	<b>63</b>	<b>32</b>	<b>1</b>	<b>2</b>	<b>2</b>	100.0	<b>36%</b>	<b>4%</b>	<b>4.8</b>	<b>12</b>	<b>1</b>	<b>4</b>	<b>14</b>	<b>2</b>	<b>0</b>	<b>6</b>	<b>0.2</b>	<b>51</b>	<b>6</b>	<b>1</b>	<b>2</b>	100.0	<b>9-16</b>
Luangwa	1	74	25	0	0	1	100.0	39%	0.3%	2.9	11	1	4	18	6	4	11	7	35	1	0	2	100.0	46
Sangara-Chacangara	2	49	48	0.3	3	0.5	100.0	44%	0.1%	3.2	4	2	0.2	4	3	0	1	0	20	41	21	4	100.0	13-24
Morrunguze	1	46	50	0	1	4	100.0	51%	1%	14.7	2	1	3	12	4	0	0	0	30	36	12	0	100.0	41
Minjova	1	70	26	1	3	0	100.0	55%	0%	0.4	6	1	1	7	25	0	0	0.5	26	24	9	0.5	100.0	91
Mufa	2	47	50	1	1	0.2	100.0	44%	1%	12.1	2	2	3	2	2	0	0.5	0	71	9	8	1	100.0	45-50
Mazowe-Luenha	2	45	53	1	0	1	100.0	38%	1%	9.0	3	1	4	12	3	0	2	1	73	1	0.5	0	100.0	31-38
<b>Lower Zambezi</b>	<b>2</b>	<b>48</b>	<b>50</b>	<b>1</b>	<b>0.4</b>	<b>0.2</b>	100.0	<b>58%</b>	<b>5%</b>	<b>16.4</b>	<b>5</b>	<b>1</b>	<b>1</b>	<b>9</b>	<b>25</b>	<b>0</b>	<b>0.2</b>	<b>0.5</b>	<b>43</b>	<b>7</b>	<b>5</b>	<b>2</b>	100.0	<b>14-63</b>
Shire	1	33	67	0	0	0.4	100.0	72%	3%	14.1	4	4	0.4	6	4	0	1	0	76	2	2	0	100.0	41
Sangadze-Zangue	2	64	35	0	1	0.2	100.0	28%	0%	1.2	2	2	1	5	58	7	4	3	18	1	0.2	0.5	100.0	27-80
<b>Lower Zambezi (final)</b>	<b>2</b>	<b>49</b>	<b>49</b>	<b>1</b>	<b>0</b>	<b>1</b>	100.0	<b>45%</b>	<b>3%</b>	<b>6.9</b>	<b>3</b>	<b>1</b>	<b>4</b>	<b>21</b>	<b>3</b>	<b>2</b>	<b>1</b>	<b>0.2</b>	<b>58</b>	<b>3</b>	<b>3</b>	<b>0</b>	100.0	<b>26-38</b>
Zambezi upper slope	3	63	35	0.2	1	1	100.0	52%	11%	3.1	4	2	4	23	3	0.2	1	3	46	11	2	1	100.0	4-7
Quelimane estuary/beaches	4	69	28	1	2	0.4	100.0	53%	2%	4.5	5	2	4	17	4	0.5	1	2	53	8	3	0.2	100.0	2-11
Quelimane outer shelf	2	58	40	1	1	0.5	100.0	46%	29%	2.2	5	3	2	24	0.2	0	0.2	4	47	14	1	1	100.0	4-8